In: Tribology and Dynamics of Engine and Powertrain: Fundamentals, Applications and Future Trends, Edited by H. Rahnejat, Woodhead Publishing, 2010, pp. 470-517, ISBN: 978-1-84569-993-2

Chapter 14
Optimised Textured Surfaces with Application in Piston-Ring/Cylinder Liner Contact

R. RAHMANI, Loughborough University, UK
A. SHIRVANI and H. SHIRVANI, Anglia Ruskin University, UK

Abstract: The application of textured surfaces in tribology has recently gained a huge momentum. In this chapter, a systematic approach to investigate the maximum outcomes from employing such surfaces is introduced with an insight into their application in internal combustion engines. A combination of various affecting parameters on the tribological performance of such surfaces is studied and the optimum results were introduced. The effect of employing such optimised textures in enhancing the lubrication condition in piston ring/cylinder liner contact is also studied.

Key words: surface texturing, piston ring/cylinder liner contact, optimisation, slider bearings

14.1 Introduction

In general, friction is inherent to and is produced between bodies in contact with relative motion. Friction tends to oppose this relative motion between the bodies through loss of energy mostly in the form of heat, mechanical vibration and noise. Therefore, in most cases, friction is an unfavourable phenomenon. In some cases introduction of friction is desired, for example in order to slow down a moving car, the brakes are used to reduce the existing kinetic energy in the wheels by means of producing frictional losses. However, in most of the cases, facilitating this relative motion between bodies is of concern and as a result, one needs to overcome friction so that the relative motion pursues with a minimal loss of energy.

Excessive friction can cause damage to the surfaces in contact in several ways and as a result make them wear. Since the surfaces are damaged due to wear, the rate of energy dissipation due to friction increases and consequently amplifies the rate of wear itself (see Chapter 2).

The reason for the existence of friction is mainly that in reality, there is no perfect smooth surface. In fact, surfaces have a degree of roughness in the form of small ‘hills’ and ‘valleys’ no matter how well they are prepared. When two surfaces, which are in contact with each other, are put into relative motion, the asperities on the

opposing surfaces become locked hence inducing friction as initially proposed by Amontons for onset of motion and later under kinetic conditions by Coulomb (see Chapter 2). Wear can ensue and as a result, the surface landscape changes and new 'hills' and 'valleys' are produced, while each time some of the material from the contacting surfaces are removed and the surfaces become worn. Some of these broken pieces can still remain in contact and produce even more resistance against the motion. As a result a form of wear, which is called ***abrasive wear***, will occur.

Therefore, the inherent roughness of surfaces can be blamed for existence of friction and occurrence of wear. However, this is not the entire story. It has been observed that, although friction can be reduced by polishing of the contacting surfaces to a very fine degree, after some point, both the friction and wear will start to increase again. The reason for this is that as the surfaces become smoother, the electromagnetic forces between molecules and/or atoms of the opposing surfaces become significant and as a results the surfaces may 'stick' to each other so that again an extra energy is required to overcome these attractive forces (see Chapter 3). However, the given energy would not necessarily break these forces evenly and as a result; some of the material from each surface will stick to the other surface. This from of wear is usually referenced as ***adhesive wear***, which is the primary cause of scuffing. Even a combination of pieces from each surface, which are attached to each other by electromagnetic forces, can be released into the contact and cause some degree of abrasive wear as well.

In practice, both of these phenomena can subsist in any contact. Here it should be noted that although there are other forms of wear that may happen in various circumstances, the two mentioned wear mechanism are considered as the major wear causes. For example, the surface may enter into a chemical reaction with each other or with environment (such as air) and as a result, ***corrosive wear*** may occur.

Since long ago, it has been discovered that introducing a third element in the contact can reduce friction and wear. These elements can keep the asperities apart from direct contact, become an insulator against intermolecular/atomic forces and protect the surfaces from chemical reactions. Such an element, usually of low shear strength is generally termed a *lubricant*.

A Lubricant can be solid, liquid or gas. Liquid lubricants, usually in the form of oils are the most common. Designing this type of lubricants involves good knowledge of rheology (see Chapters 3 and 5). The lubricating oils that are nowadays used in industry are evolved in the last century and can be mineral, organic or synthetic type. In addition, depending on application, a combination of various additives of different can be introduced in the base oil to provide a suitable lubricant.

Alongside with designing appropriate lubricants, improvements to tribological characteristics of contacting surfaces are also achieved through surface engineering. In general, surface engineering can be considered in two categories: surface coating (see Chapter 4) and surface modification (treatment) (also see Chapter 13). In surface coating technology a layer (or layers) of a material (or materials) are implanted over the main contacting surfaces in order to enhance their tribological characteristics such as wear resistance. The coating process can also be achieved by altering the chemical composition of the surface itself. Methods in which the surface is modified without changing its composition such as polishing, honing, heating or employing local melting-solidification are called the ***surface modification*** (or treatment) methods.

In recent years, efforts for better controlling of friction and wear have been focused on the modification of surface topography including parameters such as surface roughness (see Chapter 2) and skewness in a controlled manner. Surface

finishing processes, such as turning, shaving, grinding, honing and polishing generate surfaces with textures of specific topography. It is believed that creating surfaces with controlled micro-geometry can be an effective approach in improving their tribological performance.

In addition to these enhancement processes on the inherent topography of the surfaces, the idea of introducing artificial and deterministic surface micro-structures in the form of microscopic surface features, having a regular geometry and a repeatable pattern have been of increasing interest. It is believed that somehow these artificial features can be designed so that they can provide a desired tribological performance.

14.2 Surface texturing

Several mechanisms may contribute to hydrodynamic lift in bearings with parallel flat and smooth surfaces that according to the conventional theory of lubrication would produce no hydrodynamic lift due to a lack of surface gradient (see Chapters 5 and 6). These mechanisms are lubricant density change, thermal, and viscosity wedge, non-Newtonian effects, squeeze film action, eccentric rotation, wobble and bounce as well as surface roughness or waviness. Of these mechanisms, the influence of surface roughness/waviness is of interest in this chapter. It is also observed that by implementing macro/micro-surface structure(s) or irregularities in the form of asperities or cavities on one of the sliding surfaces, an additional load carrying capacity within a coherent lubricant film may be developed. These results were achieved in mid 1960s, when Hamilton *et al* (1966) at BMI, USA investigated the effect of surface irregularities on lubrication and promoting self-sustaining films in parallel rotary-shaft mechanical face seals. They examined both asperities and cavities. Their work was continued by Anno *et al* (1968, 1969). Since then, it has been recognised that micro-surface patterns, such as radial tapers, hydro-pads, lobes, and grooves can introduce beneficial effects on lubrication of mechanical seals and enhance their axial stiffness.

This concept was developed further from mid and late 1990s, mainly thanks to the works conducted by Etsion *et al* (1996, 1999). They employed laser technology to produce surface textures in the form of shallow dimples or pores.

Different terms in literature have been used to describe these artificially implanted surface features such as ***deterministically controlled textures*** (Wong *et al*, 2006) and ***intentionally created surface undulations*** (Blatter *et al*, 1999). They may also be called (macro- or micro-) surface features, structures, geometries or topographies, as well as textures. In general, these surface textures can be of two types: they may be produced by *engraving* the surface, whether in the form of an individual *spot* or a narrow *channel*. In the former case, they are usually named ***dimples***, depressions, pits, pockets, pores, indents or dents, recesses, holes or cavities in the literature. These terms are also often accompanied with adjectives such as shallow or hollow. In the latter case, they are commonly called ***grooves*** or sometimes valleys, treads, troughs or corrugations. In addition, they might be produced as protruding objects on surfaces, whether in a continuously projected line form or as an individually projected object or *spot*, which in this case are usually called, protrudes or protrusions, peaks, bumps, posts, (micro-) islands or more commonly asperities. It is also common to use the terms ***negative textures*** or ***positive textures*** to distinguish the engraved form from the protruding type textures.

Early textures were limited to grooves or troughs, while new techniques have allowed complex patterns of different shapes, including circular, triangular, and other geometric shapes, to be used. Asperity shape, geometry, depth, area ratio (the ratio of

asperity to the flat area) and orientation can all influence the tribological effectiveness of a sliding surface.

Depending on the requirements for a specific application, the depth of these dimples can range from a few to several micrometres (normally 4-10μm) and their diameter can be several tens of micrometres (normally 70-100μm) (Erdemir *et al*, 2005 and 2004b).

14.3 Application of surface texturing in tribology

Surface texturing is receiving an ever-increasing attention in tribological design as the previous studies have shown its potential to improve lubrication and reduce friction and wear. Nowadays, the concept has become common practice in some industrial applications. As an example, very small textures are employed in the *landing* sections of magnetic storage disc surfaces to prevent adhesion when the recording heads contact the surface (Wong *et al*, 2006 and Etsion, 2005). Surface texturing is also considered as a means for overcoming adhesion and stiction in the MEMS devices (Etsion, 2005).

Micro-texturing of functional tool surfaces can help reduce friction and wear during critical forming processes like cold forging (Wagner *et al*, 2006 and 2008), sheet rolling (Ike *et al*, 2002), deep drawing (Vermeulen and Scheers, 2001). This increases tool life and reduces the amount of consumed lubricants.

In recent years, great strides have also been made in the texturing of various tribological surfaces including mechanical seals (Etsion and Halperin, 2002, Yu *et al*, 2002, Yagi *et al*, 2008 and Yi and Dang-Sheng, 2008) and dry gas seals (McNickle and Etsion, 2004), thrust bearings (Etsion *et al*, 2004) or journal bearings (Lu and Khonsary, 2007), ring/liner assembly of IC engines (Ryk *et al*, 2002, Ryk and Etsion, 2006, Rahnejat *et al*, 2006 and Etsion and Sher, 2009), roller/piston contact in hydraulic motors (Pettersson and Jacobson, 2007). The textures produced on these surfaces can improve the hydrodynamic efficiency by altering the regime of lubrication or performance of sliding surfaces. Surface texturing is a cheap technology for applications in mechanical face seals to produce load carrying capacity, when compared with other methods such as spiral grooves, waviness etc. This technology has also been successfully applied to mechanical seals used in operating pumps in the field (Etsion *et al*, 1999).

A well-known example of tribological improvement through surface texturing is in automotive industry where the honing of the cylinder liners for internal combustion engines can aid support the oil retention and re-supply. Surface texturing has also been proposed to be employed in engine powertrain and drivetrain components and wrist pin bearings, where the supply of lubricant is usually rather poor, etc (Ryk *et al*, 2002, Etsion *et al*, 2006, Lisowsky, 2006 and Borghi *et al*, 2008).

14.4 Surface texturing methods

Several methods are available for creating the surface micro-topographies. Mechanical techniques such as ***vibro-rolling*** and ***abrasive machining*** can be used to create grooves (Wong *et al*, 2006). Micro-dimpling has also been achieved with AJM (abrasive jet machining) by Wakuda *et al* (2003), while using mechanical scribing through utilising a Rockwell indenter. Hsu *et al* (2003) and Krupka and Hartl (2007) have produced grooves and dimples on the metal surface. Examples of textured surfaces produced by indentation using a hardness tester can be found in Pettersson (2005), for instance.

Embossing offers the possibility to transfer a textured pattern onto all plastically deformable materials including steel (Pettersson, 2005 and Pettersson and Jacobson, 2006).

Methods including deep RIE (reactive ion etching) (Wang *et al*, 2003), different forms of etching and ***UV lithography*** can produce a variety of shapes in both metals and ceramics (Alberdi *et al*, 2004 and Wong *et al*, 2006). Early studies have used ***photo-etching*** for micro-asperity fabrication (Siripuram, 2003 and Hsu *et al*, 2003). The electrical discharge etching has also been used by Ito *et al* (2000). Using combined techniques of PVD (***physical vapour deposition***) and UV photo-lithography has been reported in the literature as well Alberdi *et al*, (2004). Costa and Hutchings (2007) have used photochemical etching, which comprises masking by photolithography followed by chemical etching. The LIGA process has been widely used in the pattern generation in silicon wafer processing, but less so in robust applications like surface texturing for tribological applications (Kortikar, 2004).

Each method has advantages and disadvantages, and some may be more appropriate for use in a given application than the other methods. For instance, etching is although flexible in producing different shapes, the process is time-consuming and the profiles of the features are determined by the chemical erosion process and cannot be controlled (e.g., round-shape textures may not be possible). Methods like photo-etching although are old traditional methods, they are limited to surfaces made of, for example, copper whilst erosion is an effective technique for hard materials (Wang *et al*, 2003). Regular and abrasive-jet machining also have some limitations on profile shape and may not be appropriate for cylinder liner texturing if machining heads are too large to access the inner liner surface (Wong *et al*, 2006). According to Wang *et al* (2003), micro-blasting is a suitable technique to produce surface texture on ceramics. The LIGA process can be used for fabricating positive asperities as well and offers an advantage of achieving higher aspect ratios. The modified photo-lithography process introduced by Kortikar (2004) is an alternative to fabricate both deterministic micro-asperities and micro-dimples with high/low aspect ratios on surface of any arbitrary cross section and orientation.

In addition to the above-mentioned methods, laser ablation or ***laser texturing*** is a new energy beam technique to achieve controlled surface textures (Andersson *et al*, 2007). Using laser material processing, topographical features on almost any material such as metal, crystalline structures and glass, ceramics and polymers can be produced (Neves *et al*, 2006, Haefke *et al*, 2000 and Etsion, 2005). The method is the most efficient and convenient approach for metals (Wang *et al*, 2003). Laser surface texturing (LST) is a flexible and high-speed texturing method that can provide well-controlled surface characteristics for a variety of materials. Examples of textured surface produced using LST technology can be found in Pettersson (2005) and Etsion (2005). By controlling the laser beam parameters, it is possible to control the diameter, depth and area density of the micro-dimples accurately.

Recent progress in laser surface texturing using focused UV-lasers has extended the possibilities for tribological surface topography modification. Excimer LBM is used by Wakuda *et al* (2003) can induce nano-to-micro-scale patterns on hard coatings such as TiN, TiCN and DLC films, utilising lasers with pico- to femto-second pulsation capability.

In general, laser-texturing technology is currently believed to be a very promising technique based on its flexibility and speed (Etsion, 2005). It is clean, environmentally friendly and provides an excellent control on the size of the dimples. However, it has a possible drawback that the laser technique may create *burrs* or

bulges of melted and re-deposited material around the edges (rims) of dimpled areas with disadvantageous tribological effects and the surfaces may require a subsequent polishing step (Wong *et al*, 2006). One of the other limitations of the laser texturing is that it can only produce dimples and of only spherical and conical shapes. In addition, using this method, the average pore depth can be produced is around 1-30μm and the pore diameter is limited to 95-230μm and at lowest aspect ratios of 0.004-0.3 (Kortikar, 2004). The concerns about heat affected zone and resulting cracks on the surface are other issues, which should be considered.

14.5 The mechanisms behind tribological improvements through surface texturing

Both the need to reduce friction and increase the load carrying capacity in bearings requires an effective lubrication strategy for sliding surfaces. Surface texturing can provide such a benefit in a number of ways. In this regard, several physical mechanisms are proposed to describe the potential effect of the micro-features.

The micro-structures in the form of intentionally created undulations or minute cavities, grooves or valleys in the surface can prohibit wear debris by entrapping (accommodating) them, whether the contact is dry or lubricated. They suppress abrasion and ploughing friction and third-body wear, resulting in improved fretting fatigue resistance, longer durability and hence reliability. This is very common idea amongst different researchers such as Blatter *et al* (1999), Fenske *et al* (2003), Alberdi *et al* (2004), Erdemir *et al* (2004a and b), Kovalchenko *et al* (2005), Etsion (2005), Wong *et al* (2006), Andersson *et al* (2007), Costa and Hutchings (2007), and Krupka and Hartl (2007).

In addition, these surface micro-structures can act as lubricant micro-reservoirs or the so-called lubricant (micro-) pockets or *lubricant capacitors* in order to improve localised lubrication by retaining the lubricant in desired locations (Blatter *et al*, 1999, Etsion, 2005, Wong *et al*, 2006 and Krupka and Hartl, 2007). These features can retain lubricant to release when needed, thus increasing the quantity of the lubricant locally even under high pressures (Blatter *et al*, 1999, Fenske *et al*, 2003, Alberdi *et al*, 2004, Uehara *et al*, 2004, Mourier *et al*, 2006 and Andersson *et al*, 2007). The liquid trapped in the low valleys of the textured surfaces can be considered as a secondary source, which is then drawn by the relative movement of the surfaces to seep into the surrounding areas by capillarity action, and therefore, reduce friction and reduce the chance of galling (Wang *et al*, 2001 and 2003). They can also transport lubricant to a desired location and subsequently expel it into the contact, resulting in much longer life for lubrication (Haefke *et al*, 2000 and Kovalchenko *et al*, 2005).

These mechanisms are thought to be important under boundary or starved lubrication conditions (Hupp, 2004 and Etsion, 2005). A normal ground surface roughness does not effectively entrap lubricant or wear debris since there is no physical mechanism by which the lubricant can be *held* in place. Therefore, an *ideal* surface texture should consist of a nearly uniform array of microscopic depressions each having geometrical dimensions similar to those of its neighbours (Haefke *et al*, 2000).

In instances where there are frequent start/stop operations, it is thought that the lubricant remaining in the pores can avoid an abnormal temperature rise caused by dry running conditions (Wakuda *et al*, 2003). Experimental results also indicate that surface texture helps the running-in progress to smoothen the contact surfaces and reduce friction (Wang *et al*, 2006).

At sufficient density, the surface irregularities can improve the wetting of the surface by lubricant, and thereby support the formation of a lubricating film. At higher sliding speeds and with a sufficient supply of lubricant, surface cavities can take action as hydrodynamic pressure sources to produce hydrodynamic fluid lift and reduce friction, unless the benefit is counteracted by turbulence or cavitation at the cavities (Kovalchenko *et al*, 2005 and Andersson *et al*, 2007).

It is suggested that during the initial stages of sliding, the leading edge of each asperity becomes slightly worn so that it acts as an inclined surface that promotes hydrodynamic lift (Hupp, 2004). In this regard, each micro-dimple acts as a micro-hydrodynamic bearing to enhance lubrication even in the partial lubrication condition (Wang and Zhu, 2005 and Etsion, 2005). This leading edge hypothesis is also supported by experimental data that indicate the initial friction at the start up is much higher than the average values (Hupp, 2004). Another hypothesis on the working mechanism of the micro-features is based on occurrence of cavitation. According to this hypothesis, an asymmetric hydrodynamic pressure distribution over each dimple owing to the *local cavitation* in the diverging clearance of the dimple provides a significant amount of load carrying capacity. Generally, the pressure increases in the converging film regions, while it decreases in the diverging film regions for incompressible fluids. The cavity generated in the diverging film regions is, theoretically, an isobaric region. The pressure in this region cannot be lower than the cavity pressure, which is the fluid vapour pressure or the pressure at which the lubricant is saturated with the gas dissolved in it. As a result, the pressure rise in the converging film regions can be much larger than the pressure drop in the diverging film regions and so additional load capacity is generated (Wang *et al*, 2001 and 2006). This type of enhancement in the load support by a hydrodynamic effect is often called ***micro-hydrodynamics*** of surface features (Mourier *et al*, 2006 and Wong *et al*, 2006).

Surface texturing can have a significant beneficial effect by increasing the boundaries of hydrodynamic lubrication. In this case, the performance improvement is thought to result from the increased hydrodynamic efficiency of such a sliding surface under the boundary-lubricated sliding condition (Erdemir, 2005). In addition to these, ***micro-plasto-hydrostatic*** lubrication effects (Hsu *et al*, 2005) and reduction of stiction owing to the smaller *real* contact area (Wang *et al*, 2006) are also enumerated as beneficial outcomes from the action of textured surfaces. The former is related to application of laser texturing in metal forming in which the micro-features act as ***micro-pools*** or a micro-plastic hydrodynamic tool (Etsion, 2005) and the latter is associated with hard disk memory devices.

14.6 Debates surrounding surface texturing

Despite the considerable emphasis in some literature put on the tribological benefits and advantages associated with surface texturing, there are some considerations and debates as well. In fact, despite of a reported decrease in friction and wear between two sliding surfaces through use of textured surfaces, some experimental results also show negative effects on contact lubrication and durability (Wong *et al*, 2006 and Mourier *et al*, 2006). Andersson *et al* (2007) point out to a drawback of the surface irregularities being abrasive wear of a soft counter-surface at high contact pressures. In addition, experimental works by Erdemir *et al* (2004a) has verified that dimpled surfaces work extremely well under mixed or hydrodynamic sliding regimes of lubrication. However, under boundary lubricated sliding conditions (i.e. high load and low speed conditions) they only provide marginal improvements in friction, but may cause increased wear losses. Hsu (2004a) also confirms that the

ability of micro-texturing to reduce friction does not seem to be effective under boundary regime of lubrication. Under these conditions, the edge stresses around the dimples increase friction rather than decrease it.

The behaviour of textured surfaces can be quite variable. Some studies show a substantial reduction in coefficient of friction due to surface texturing (e.g. Aldajah *et al*, 2005), while others report virtually no difference between textured and untextured surfaces (e.g. Pettersson and Jacobson, 2003). Sometimes texturing is not optimised for a given case, in others there is no optimal case and any kind of texturing may be worse than a nominally smooth surface (Wong *et al*, 2006). For example, some studies show that surface texturing can reduce friction only if the pattern features are smaller than the contact width (e.g. Wang *et al*, 2001 and Pettersson, 2005), while others show that friction increases under these conditions (e.g. Wakuda *et al*, 2003). The extent of the reported effect has also been variable (Costa and Hutchings, 2007). In some tests, adding texturing can increase friction or have no effect on the friction coefficient, but the mechanism is not clear (Hsu *et al*, 2003, and Blau and Qu, 2004). Whilst some studies have shown that texturing removes wear particles from a sliding interface, a good understanding of the chemical interaction of the materials involved in sliding is required to predict the possible effects on friction. For instance, Kovalchenko *et al* (2005) have observed that, when the dimples are relatively deep or when the oil viscosity is relatively high, LST might be detrimental to tribological performance under starved lubrication conditions.

Nevertheless, despite the above-mentioned facts, the use of surface texturing has opened a new avenue to explore friction reduction especially in engine applications. Research and analysis presented to date demonstrates both the potential to improve tribological properties via surface texturing, and the need to understand materials, lubricants and running conditions before a surface texture is applied (Wong *et al*, 2006). According to Hsu *et al*, (2005), there is lack of theory and understanding in designing of these features and the mechanism(s) and set of conditions in which these features can influence friction and durability. Detailed mechanisms of friction reduction are not fully understood and the lubrication phenomena induced by the micro-geometry distribution remain widely unknown (Mourier *et al*, 2006). Moreover, the influence of size and shape of the surface texture on their tribological performance is not well known either (Alberdi *et al*, 2004). In fact, the maximum benefits that can be accrued from sophisticated texturing are unclear and this area is relatively unexplored.

According to Hsu (2004b), the effect of dimples on friction reduction appears to depend on textures' size, their pattern and density on the contacting surfaces. The dimensions and area ratio of the textures are considered as important parameters related to the generation of hydrodynamic pressures (Wang *et al*, 2006). Surface texture shape and orientation may also have a significant effect on friction and especially wear (Hsu, 2004a and b). On the other hand, Ronen *et al* (2001) and Ryk *et al* (2002) point out that the main geometrical parameters of laser texturing, which can affect friction, are the ratio of dimple depth to its diameter and the area density of the dimples.

As Wong *et al* (2006) mention that the outcome of research works to date indicates that optimal surface texturing parameters depend on the running conditions and on the dominant regime of lubrication. Each optimisation process requires an accurate correlation of the micro-geometry dimensions and density with its induced lubrication influence for the relevant range of operating conditions, which is still difficult to obtain as noted by Mourier *et al* (2006). Hence, the fundamental

understanding of the lubrication phenomena induced by a single micro-feature, as a function of its dimensions and the operating conditions is an important step.

Reviewing the literature, indicates that there is no general agreement on the related issues such as what types of textures should be used and under what conditions. In addition, there is no general agreement on what texturing parameters are the most important in friction reduction or load support and even what the effects of various texture parameters may be. For instance, the results from Kovalchenko *et al* (2005) show a better performance for textured surfaces in boundary and mixed lubrication condition, whilst almost no improvement in hydrodynamic lubrication conditions ensue. On the other hand, the results from Etsion *et al* (2004) show a 50% reduction in friction by applying micro-textures in hydrodynamic regime of lubrication.

As another example, Hsu *et al* (2005) state that in high-speed, low-load conditions, surface feature shape and size has great influence on friction reduction, whilst Etsion *et al* (1999), under almost same conditions, reveal that the actual shape of the micro-dimple is insignificant. Pettersson and Jacobson (2003) observed no improvement by laser texturing in dry and lubricated cases and Blau and Qu (2004) under dry condition, whilst according to the majority of literature it is believed that even in these conditions, the textured surfaces can be beneficial by trapping wear debris and reducing friction as a result. In addition, the results of Aldajah *et al* (2005) show lower coefficients of friction for textured surfaces when compared with untextured ones for a whole range of boundary to mixed and early hydrodynamic regimes of lubrication. According to Hupp (2004) and Petterson (2005), the surfaces with a higher percentage of surface area taken up by micro-pores have a lower coefficient of friction under the hydrodynamic and mixed regimes of lubrication regimes, whilst Wang *et al* (2001, 2003) propose a very small area ratio for pores as the optimum case.

Through the published experimental research, one cannot reach a specific conclusion. For example, in the work by Blatter *et al* (1999) although the distance between grooves is kept constant, it is not known that the better performance of the *finer* grooves is due to their smaller width or due to their shallower depth. Furthermore, study of the literature shows a lack of systematic approach in the study of the textured surfaces and the corresponding optimisation procedures. As Etsion (2005) also confirms, a trial and error approach is adopted whenever optimisation of the texturing dimensions is attempted. Consequently, a relatively large range of optimum parameters has been attained in different studies.

Of course, this trial and error approach in some cases is the only option in the study of the performance of textured surfaces such as dry or boundary lubrication conditions, where there is a lack of basic theoretical modelling approach. However, in the rest of the cases such as under hydrodynamics, there is a considerable theoretical basis. Nevertheless, even in these cases, there remains a lack of a general and systematic optimisation approach and a few efforts have been reported, largely through numerical trial and error (e.g. Brizmer *et al*, 2003). As Wong *et al* (2006) suggest, much work yet remains in this field before a good understanding of the effects of surface texturing is achieved.

14.7 Surface texturing technology and internal combustion (IC) engines

The frictional losses in IC engines are an important factor in influencing fuel economy and performance of vehicles. Estimates show that nearly 40 to 50% of the

total frictional losses of an IC engine are due to the piston/cylinder system of which 70 to 80% are attributed to the piston rings (Ronen *et al*, 2001 and b, Ryk *et al*, 2002 and Ryk and Etsion, 2006). Reducing these frictional losses is a key factor in reducing fuel consumption and protecting the environment. In addition, the internal combustion engine contributes to environmental pollution through particulate, NOx, HC and to the greenhouse effect via CO_2 emissions (Taylor and Coy, 2000 and Tung and McMillan, 2004).

Improving fuel efficiency of IC engines, while still enabling them to meet environmental requirements, presents both design and material challenges. Reducing parasitic frictional losses in engines can be achieved by a combination of strategies such as those noted by Blau and Qu (2004):

- redesigning the engine components
- reformulating the lubricants
- improving methods of lubricant filtration and supply
- reducing churning losses in fluids
- changing the operating conditions of the engine
- substituting more durable, low friction materials
- altering the finish or micro-scale geometry of the bearing surfaces

Among these factors, proper lubrication and surface roughness are key issues in reducing friction in the piston/cylinder system. Improvement to surface finish is one of the most reasonable methods for friction reduction. This has therefore, promoted an increase in the number of automotive components whose surfaces are finished with grinding with subsequent additional processes such as lapping or super-finishing. However, the attainable surface roughness is ultimately limited by the material and machining considerations. The earliest and well-known industrial application of effective surface treatment in the automotive industry is of course cylinder liner honing.

On the other hand, surface texturing can be regarded as another striking approach for elements subjected to sliding contact. This area of research is widely unexplored and needs an extensive research (Hsu, 2004b). Although the textured surfaces have shown the potential to reduce friction under reciprocating sliding conditions, there is a lack of agreement over the underlying mechanism(s) involved and the optimum condition with which maximum benefits can be accrued (Wong *et al*, 2006).

Overall, it is expected that by producing optimised textures on various engine and drive train components, a great deal of improved fuel economy would be achieved due to subsequent reductions in friction, gaining longer durability and hence reliability through suppression of wear.

14.8 The basic equations of tribology

14.8.1 The Reynolds hydrodynamic lubrication equation

As is common in tribology of bearings in general, the Reynolds hydrodynamic lubrication equation is used for the analysis the textured surfaces as well.

Reynolds equation can be derived either by writing the equilibrium equations for an infinitesimal element inside the lubricant film and considering the mass continuity equation (e.g. Stachowiack and Batchelor, 2001) or by simplifying the Navier-Stokes (N-S) equations considering a series of assumptions (e.g. Pinkus and Strenlicht, 1961). It can also be obtained rather simply through dimensional analysis

In: Tribology and Dynamics of Engine and Powertrain: Fundamentals, Applications and Future Trends,
Edited by H. Rahnejat, Woodhead Publishing, 2010, pp. 470-517, ISBN: 978-1-84569-993-2

of fluid flow (Gohar and Rahnejat, 2008). The derivation of Reynolds equation is carried out in Chapter 5.

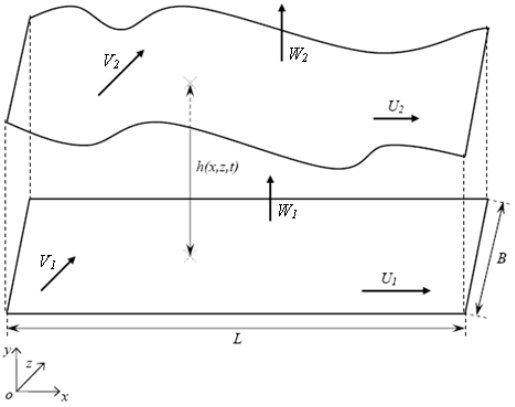

Figure 14.1: An arbitrary bearing geometry

Consider Figure 14.1 for an arbitrary bearing geometry, a general form of Reynolds hydrodynamic equation in 2D/3D form for an arbitrary reference point in space in the Cartesian coordinate system may be stated as follows:

$$\frac{\partial}{\partial x}\left[\frac{\rho}{\eta_0}\left(\frac{\partial p}{\partial x}\right)(h_2-h_1)^3\right]+\frac{\partial}{\partial z}\left[\frac{\rho}{\eta_0}\left(\frac{\partial p}{\partial z}\right)(h_2-h_1)^3\right]=12\rho(W_2-W_1)$$
$$+6\left\{\rho(U_1+U_2)\frac{\partial}{\partial x}(h_2+h_1)+(h_2-h_1)\frac{\partial}{\partial x}\left[\rho(U_1+U_2)\right]\right\} \qquad (14.1)$$
$$+6\left\{\rho(V_1+V_2)\frac{\partial}{\partial z}(h_2+h_1)+(h_2-h_1)\frac{\partial}{\partial z}\left[\rho(V_1+V_2)\right]\right\}$$

In this equation, the second and the third terms on the right hand side are called the wedge terms (or Couette flow terms), whilst the first term on the right hand side is called the squeeze film term. Wedge terms correspond to the flow due to surface velocities, whilst the squeeze film term accounts for flow into the contact due to lubricant entrapment by mutual approach of surfaces. The pressure build-up is due to changing of film thickness with time (Lubbinge, 1999). In the latter case, changes in the film thickness can be induced indirectly because of variations of the sliding velocity (wedge term) or it can be caused as a direct consequence of variations in the normal velocity of the bearing surface(s).

It is noted that since in the given equation the pressure distribution in the *y*-direction is neglected, therefore it can be considered as a 2D equation. On the other hand, since this equation is capable of taking into account the variations of surface geometry and clearance between the mating surfaces, which are stated in the *y*-direction, therefore it can be considered as a 3D equation. Thus, it is more convenient to use the terms ‘quasi-3D’ or ‘2D/3D’ for the given equation.

The Reynolds equation in general form stated in equation (14.1). It is often somewhat simplified to represent a specific problem. By considering the coordinate system attached to the bottom surface, then h_1=0 and h_2=h. The squeeze film term is also usually specified based on the variations of the distance between bearing surfaces with time; i.e. W_2-W_1=$\partial h/\partial t$. In addition, the transversal sliding components can also be neglected in the most of engineering problems, i.e. V_1=V_2=0. Furthermore, it can be assumed that the bearing surfaces are inelastic in the *x*-direction (Pinkus and Strenlicht, 1961); i.e. $\partial(U_1+U_2)/\partial x$=0. In addition, if the lubricant is considered an

incompressible and an isoviscous fluid, which results in $\partial\rho/\partial x=\partial\rho/\partial z=0$ and $\partial\mu/\partial x=\partial\mu/\partial z=0$, respectively, the Reynolds equation can be downsized as follows:

$$\frac{\partial}{\partial x}\left[h^3\left(\frac{\partial p}{\partial x}\right)\right]+\frac{\partial}{\partial z}\left[h^3\left(\frac{\partial p}{\partial z}\right)\right]=6\eta_0\left(U_1+U_2\right)\frac{\partial h}{\partial x}+12\eta_0\frac{\partial h}{\partial t} \tag{14.2}$$

It is noted that the general Reynolds equation in 2D/3D form is an elliptic second-order PDE with respect to pressure. In the 1D/2D though, the Reynolds equation turns into a non-complete second-order linear non-homogenous variable coefficient ODE with respect to pressure.

The load carrying capacity of a bearing can be calculated through integrating the obtained pressure distribution over the bearing profile. In addition, the total (viscous) friction force for each surface is obtained from calculating the (viscous) shear stress based on the velocity profile inside the film. Hence, the friction coefficient can be obtained based on the well-known Amonton or Coulomb's law as follows:

$$\eta=\frac{F_v}{W_H}=\frac{\int_0^B\int_0^L\left[\pm\left(\frac{\partial p}{\partial x}\right)\frac{\left(h_2-h_1\right)}{2}+\frac{\eta_0\left(U_2-U_1\right)}{h_2-h_1}\right]dxdz}{\int_0^B\int_0^L pdxdz} \tag{14.3}$$

where, the negative sign is used for the lower surface and positive sign for the upper.

Lubricant flow rate inside the bearing can be another interesting parameter in order to analyse the bearings under hydrodynamic regime of lubrication. It is defined as (see Chapter 5):

$$Q_x=\int_0^B\left[-\frac{1}{12\eta_0}\left(\frac{\partial p}{\partial x}\right)\left(h_2-h_1\right)^3+\frac{1}{2}\left(U_1+U_2\right)\left(h_2-h_1\right)\right]dz \tag{14.4}$$

A similar type of equation can also be obtained for the lubricant flow rate in the transversal direction.

14.8.2 Bearing dynamics equation

When analysing the bearings, one may often come across situation(s) where the bearing surfaces are under external loads as well. These loads can be constant or variable with time and both types may exist at the same time originating from various sources. A good example of this is the case of piston-ring/cylinder liner contact, where the ring is under constant and variable loads. In addition, the generated hydrodynamic load capacity by the ring is variable too due to its reciprocating motion. The dynamics of the ring in its retaining groove can be modelled by considering the forces acting on a section of the ring.

By neglecting ring twist, Figure 14.2 illustrates the forces exerted on a piston ring in the top ring groove of a gasoline engine (see Barrell *et al*, 2000). Applying Newton's second law of motion in the axial and radial directions gives:

$$\begin{cases} m\dfrac{d^2x}{dt^2}=R_G+F_a+F_v-P_A-W_g \\ m\dfrac{d^2y}{dt^2}=P_R+T+F_G-P_U-P_L-W_H-W_a \end{cases} \tag{14.5}$$

Since the variations of oil film thickness with time, i.e. $\partial h/\partial t$, is of concern; therefore, the dynamics of the ring in the radial direction is more of interest. If,

$$F=P_R+T+F_G-P_U-P_L-W_a \tag{14.6}$$

and allowing the coordinate system to be on the cylinder liner with *y*-axis facing the ring and replacing *y* with the minimum clearance or film thickness, h_m, the second equation in (14.5) can be written as follows:

$$m\frac{d^2h_m}{dt^2} = W_H - F \tag{14.7}$$

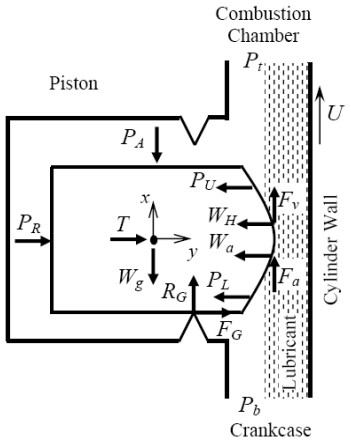

Figure14.2: Forces diagram on a piston ring in an IC engine (Barrell *et al*, 2000 and Priest and Taylor, 2000)

14.9 Modelling of the textured surfaces

14.9.1 Terminology of the textured surfaces

In Figure 14.3, the following dimensionless parameters may be defined in order to describe the geometry of the textured surface:

- Leading edge length - to - bearing length ratio (leading length ratio) for both *x*- and *z*-directions:

$$\alpha_x = \frac{a_x}{L} \text{ and } \alpha_z = \frac{a_z}{B} \tag{14.8}$$

- Trailing edge length-to-bearing length ratio (trailing length ratio) for both *x*- and *z*-directions:

$$\beta_x = \frac{b_x}{L} \text{ and } \beta_z = \frac{b_z}{B} \tag{14.9}$$

- The area density of textures in *x*- and *z*-directions:

$$Sp_x = \frac{d_x}{l_x} \text{ and } Sp_z = \frac{d_z}{l_z} \tag{14.10}$$

- The (general) area density of textures:

$$Sp = \frac{A_d}{l_x \cdot l_z} \tag{14.11}$$

  in which, A_d denotes the surface area of the base of an individual texture and the denominator is the surface area of an imaginary rectangular cell around the texture as is defined in Brizmer *et al* (2003).

- The ***texture height ratio***:

$$\xi = 1 + \frac{h_d}{h_m} \tag{14.12}$$

- *Textured area ratio* (textured portion):

$$\kappa = \frac{\left[L-\left(a_x+b_x\right)\right]\cdot\left[B-\left(a_z+b_z\right)\right]}{L\cdot B} = \frac{\left[N_x d_x+\left(N_x-1\right)l_x\right]\cdot\left[N_z d_z+\left(N_z-1\right)l_z\right]}{L\cdot B} \quad (14.13)$$

- The aspect ratio for the base of texture feature:

$$\varphi_d = \frac{d_x}{d_z} \quad (14.14)$$

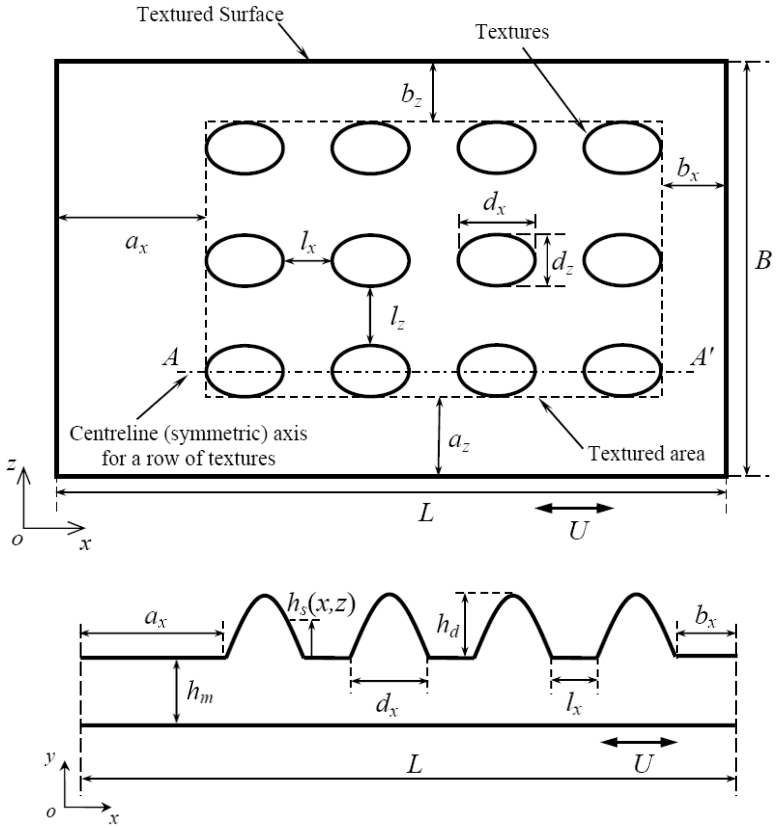

Figure 14.3: Schematic of a textured bearing surface and the **corresponding geometrical parameters**

14.9.2 The associated dimensionless groups and the dimensionless form of the equations

Non-dimensionalising of the time-independent Reynolds equation

If the bearing length, L, minimum clearance between the bearing surfaces, h_m, and the ambient pressure, P_a, are considered as the reference length, height and pressure, respectively; the dimensionless length, width, height and pressure can be defined as (see Figure 14.3):

$$x^* = \frac{x}{L}, \quad z^* = \frac{z}{B}, \quad h^* = \frac{h}{h_m}, \quad p^* = \Lambda\left(\frac{p-P_a}{P_a}\right) \quad (14.15)$$

in which, Λ is the *bearing number* defined as:

$$\Lambda = \frac{P_a h_m{}^2}{\eta_0 UL} \quad (14.16)$$

By defining the *bearing aspect ratio* in the xz-plane as $\varphi=B/L$, the dimensionless steady Reynolds equation becomes:

$$\frac{\partial}{\partial x^*}\left(h^{*3}\frac{\partial p^*}{\partial x^*}\right)+\left(\frac{1}{\varphi}\right)^2\frac{\partial}{\partial z^*}\left(h^{*3}\frac{\partial p^*}{\partial z^*}\right)=6\frac{\partial h^*}{\partial x^*} \tag{14.17}$$

In addition, the dimensionless load capacity, friction force and lubricant flow rate in the *x*-direction can be written as:

$$W_H{}^* = \frac{(W_H - P_a LB)h_m{}^2}{\eta_0 UL^2 B}, \quad F_v{}^* = \frac{F_v h_m}{\eta_0 ULB}, \quad Q_x{}^* = \frac{Q_x}{UBh_m} \tag{14.18}$$

Note that the term $\eta_0 ULB/h_m$ is in fact the friction force for a bearing with parallel and smooth flat surfaces in the absence of any pressure difference between bearing ends. In addition, the lubricant flow for such a case would be $UBh_m/2$. Therefore, the absolute dimensionless friction force and lubricant flow for such a bearing in the absence of pressure difference between bearing ends would be 1 and 1/2, respectively (Rahmani, 2009).

The *modified* friction coefficient based on the dimensionless load capacity and friction force can also be defined as:

$$\eta' = \frac{F_v{}^*}{W_H{}^*} \tag{14.19}$$

Non-dimensionalising the time-dependent Reynolds equation

The transient Reynolds equation is expressed in dimensionless form using some different (forms of) non-dimensionalising parameters than it was used before in the steady state case. The main reason is the presence of the new parameter; time, and having a variable minimum film thickness and sliding velocities, which can take different values including zero (specially for the latter case) and hence, cannot appear in (the denominators of) the non-dimensional groups defined in the steady state analysis. The dimensionless time and pressure are defined as:

$$t^* = t\frac{P_a}{\eta_0}, \quad p^* = \left(\frac{p - P_a}{P_a}\right) \tag{14.20}$$

In the transient analysis, the film thickness in the general form, $h=h(x,z,t)$, can be decomposed into two spatial and temporal components as follows:

$$h(x,z,t) = h_m(t) + h_s(x,z) \tag{14.21}$$

Since in the transient analysis, the temporal term is variable, therefore, it cannot be chosen for non-dimensionalisation. For this reason, an arbitrary parameter such as the bearing length can be considered as a suitable parameter for this purpose:

$$h^* = \frac{h}{L} \tag{14.22}$$

To obtain a relation for the sliding velocity, consider the case of a piston-cylinder mechanism in the IC engines as schematically shown in Figure 14.4. If the crank angle is assumed to be zero when the piston is at TDC, the sliding velocity of piston at each crank angle can be expressed as follows:

$$v_p = \dot{s} = -r\omega\sin\theta\left(1+\lambda\frac{\cos\theta}{\sqrt{1-\lambda^2\sin^2\theta}}\right) \tag{14.23}$$

Considering that $\theta=\omega.t$, and by defining the ***transient bearing number*** as

$$\Lambda_\omega = \frac{\eta_0\omega}{P_a} \tag{14.24}$$

the dimensionless form of the time-dependent Reynolds equation can be written as:

$$\frac{\partial}{\partial x^*}\left(h^{*3}\frac{\partial p^*}{\partial x^*}\right)+\left(\frac{1}{\varphi}\right)^2\frac{\partial}{\partial z^*}\left(h^{*3}\frac{\partial p^*}{\partial z^*}\right)=6\Lambda_\omega r^*\Xi\left(t^*\right)\frac{\partial h^*}{\partial x^*}+12\frac{\partial h^*}{\partial t^*} \tag{14.25}$$

in which:

$$r^*=\frac{r}{L} \tag{14.26}$$

and

$$\Xi\left(t^*\right)=-\sin\left(\Lambda_\omega t^*\right)\left(1+\lambda\frac{\cos\left(\Lambda_\omega t^*\right)}{\sqrt{1-\lambda^2\sin^2\left(\Lambda_\omega t^*\right)}}\right) \tag{14.27}$$

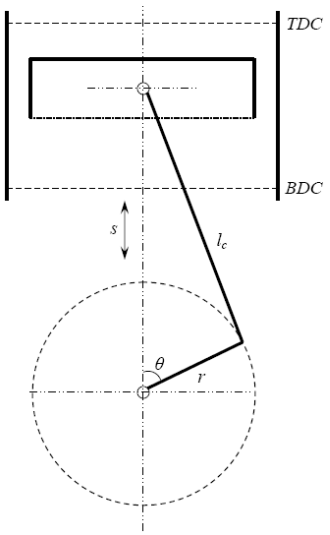

Figure 14.4: Schematic of a piston-cylinder mechanism

Non-dimensionalising of the ring dynamic equation

The dynamic equation for a typical piston ring given in equation (14.7) can also be expressed in the dimensionless form as:

$$\Lambda_M\frac{d^2h_m^*}{dt^{*2}}=W_H^*-F^* \tag{14.28}$$

in which:

$$W_H^*=\frac{W_H}{P_aBL}\ \text{and}\ F^*=\frac{F}{P_aBL} \tag{14.29}$$

and Λ_M is called the dimensionless inertia parameter, defined as follows:

$$\Lambda_M=\frac{mP_a}{\eta_0^2B} \tag{14.30}$$

Finally, the dimensionless *squeeze velocity* may also be defined as follows:

$$W^*=\frac{\eta_0W}{P_aL} \tag{14.31}$$

14.10 Solution methods

14.10.1 Analytical approach

Knowing the profile of the bearing surfaces, the steady state Reynolds equation can be solved analytically by employing full-Sommerfeld or ***Gumbel***

boundary conditions. However, the obtained results are of no practical importance when cavitation occurs. For example, an analytical solution for a barrel-shaped piston ring profile obtained using full-Sommerfeld boundary conditions shows the existence of no net hydrodynamic load support, whilst the experiments have shown that such a surface profile can develop significant load carrying capacity. Therefore, to obtain valuable results, the cavitation boundary conditions must be employed. However, since in the given cavitation models, the rupture point is not already known, implementing these models in an analytical solution would not be a very easy task, especially if the surface profile has a complex geometry. Despite this, an example of an analytical solution for a parabolic bearing surface profile, considering Reynolds-Swift-Stieber (RSS) cavitation boundary condition can be found in Rahmani (2009).

One of the main interests for developing the analytical solution methods for the textured slider bearings is the computation times' considerations associated with the numerical approaches, especially when the number of texture features grows. In the case of textured surfaces, the numerical mesh inside each single texture should be sufficiently dense to capture the surface profile gradient appropriately. In addition, an appropriate meshing scheme should also be employed for the *edge areas* of features, where the textured profile meets the bearing surface. Of course, for a bearing with a large number of textures this will cause the numerical approach to be very time-consuming. This problem may escalate when the optimisation of textured surfaces is of concern as the common optimisation approaches may need considerable number of the cases to be evaluated.

Another main concern with the numerical approach is that special means should be considered in order to tackle the cases, where the texture profile has a sharp edge, such as those, which may appear in a rectangular shaped texture, implanted on a slider bearing with parallel flat surfaces. This may also increase the time penalty of the numerical approach.

For surfaces with geometrical (profile) discontinuities such as those that comprise a number of regular textured patterns, an analytical approach has been introduced by Rahmani *et al* (2007). The method has been developed in Rahmani *et al* (2010) to include any given texture profile either in negative or positive form. The given analytical relations in Rahmani *et al* (2010) for some texture profiles can be used for the cases where the texturing pattern and/or pressure boundary conditions are such that cavitation is not a dominant phenomenon. It is also shown that the given approach can be employed for the surfaces with asymmetric texturing patterns with satisfactory results. Pascovici *et al* (2004, 2009) have also attempted to produce analytical solutions for the problem of partial textured surfaces.

14.10.2 Numerical approach

The finite difference method is a common approach in order to discretise the governing Reynolds equation. The obtained system of linear algebraic equations can be solved by direct decomposition methods such as Gauss, Choleski and LUD methods (Booker, 1988, see also Chapter 19). However, indirect iteration methods are the most common. In the iterative approach, starting from the initial condition given for pressure (e.g. ambient pressure), in each iteration step, the pressure at each node is calculated using the pressures at its neighbourhood found from the previous iteration. This is called the ***Jacobi iteration method***. However, the convergence rate can increase by 100% if the current values of the dependent variable are used to compute the neighbouring points as soon as they are available (Hoffmann and Chiang, 1993). This method is acknowledged as the ***point Gauss-Seidel iteration*** method. In

addition, the solution can be accelerated using a method called ***point successive over-relaxation*** (PSOR) or simply ***successive over-relaxation*** (SOR) technique (see various Chapters 6, 17, 20).

Implementation of the Reynolds cavitation boundary condition into the numerical computations is very simple and straightforward. For iterative solution methods, the Christopherson method is employed (Christopherson, 1941). In this method the linear equation set obtained by discretising of the Reynolds lubrication equation is solved by employing the desired numerical iterative method (see next section), in which case after each iteration step, any computed pressures lower than the cavitation pressure are set equal to the cavitation pressure and the process is repeated until satisfactory convergence is achieved.

In the 2D/3D analysis, determining of the boundary conditions at the bearings laterals are also of demand. In this case, determining the boundary conditions is completely problem dependent. In general, two assumptions can be made. In the first assumption, it is supposed that the bearing has a finite width. Therefore, the leakage from bearing laterals should be considered. In this case, the boundary conditions are of Dirichlet type, where the pressures at the leading and trailing edges in the transversal direction (i.e. z-direction) (or lateral edges) are set to the desired pressure values. It should also be noted that in this case, the textures on the bearing surface (if it is textured) could be considered with either finite width (i.e. pores or asperities) or infinite width (i.e. grooves in either positive or negative form). In the second assumption, it is supposed that the bearing has infinite width. Therefore, if the bearing is either textured with parallel positive or negative grooves or not textured, the problem can be simplified to a 1D/2D model. However, if the bearing has finite width textures such as pores or asperities, then the problem is still in 2D/3D form. In this case and, the condition at the transversal (lateral) leading and trailing edges are considered periodic spatially, where the pressure gradient is set to be equal to zero at these boundaries, and hence, the boundary conditions are the specific form of the Neuman type boundary conditions.

Both of these assumptions can be of interest in the study of the textured surfaces. For example, if the numerical analyses attempt to model the behaviour of the textured surfaces being tested experimentally on a tribo-testrig, where two finite size flat surfaces are sliding against each other, then the application of the first assumption seems to be more reasonable. However, if the numerical analyses are intended to simulate the conditions (e.g. between piston ring and cylinder liner in an engine), then due to symmetry of the ring profile in the circumferential direction, the second assumption for the lateral boundary conditions may be more realistic.

14.11 Optimisation of textured surfaces

14.11.1 Parameters involved in the optimisation of textured surfaces

In a broad spectrum, there are relatively considerable amounts of parameters that may alter the performance of a textured bearing in practice. Therefore, it is very important to address these parameters before any attempt is made for their optimisation. A list of parameters that in any modelling approach are given as follows (Rahmani, 2009):

- The profile of the surface(s) that will host the textures. This is one of the most important parameters. So far, most of the numerical analyses have focused on the textured bearings with parallel flat surfaces. Figure 14.5a demonstrates a

series of textures implanted on a flat surface, whilst the case for a curved surface such as a barrel-shaped piston top ring is shown in Figure 14.5b.

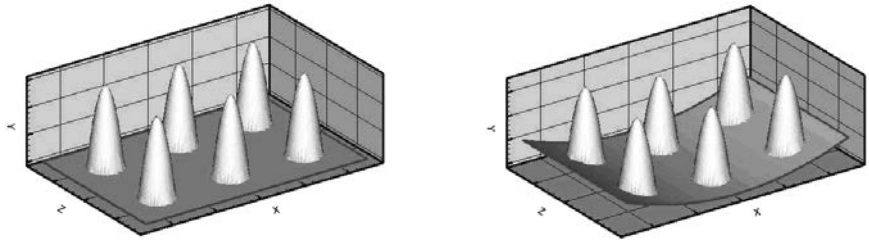

(a) **(b)**

Figure 14.5: A 3D representation of textured (a) flat and (b) parabolic bearing surface profiles

- 1D/2D or 2D/3D bearing profile assumption: In the former, the textures are considered infinite in width such as grooves and in the latter; the textures may be considered with finite width such as pores. Figure 14.6a represents a schematic of textured bearing with infinite width textures, whilst in Figure 14.6b a series of textures with finite width are shown. Note that the finite width textures can still be considered on an infinite width bearing. In this case, a symmetrical boundary condition approach may be used in the lateral direction.

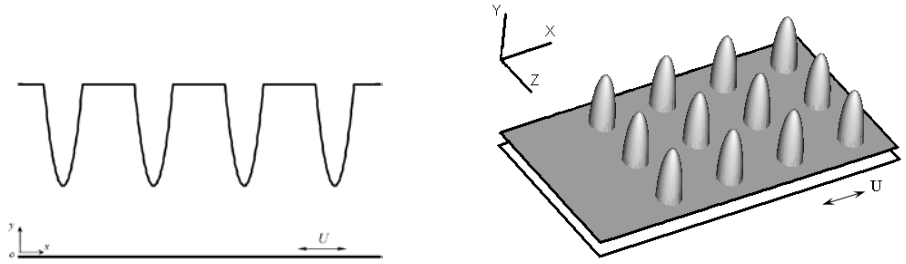

(a) **(b)**

Figure 14.6: Schematic of a (a) 1D/2D model of a textured bearing with infinite width textures and a (b) 2D/3D model of textured bearing surface with finite with textures

- Arrangement of textures on the bearing surface or the textured pattern: In general, three main arrangements of textures on a bearing surface can be considered including asymmetric partially textured, symmetric partially textured and fully textured patterns, which are shown in Figure 14.7a, b and c for 1D/2D configurations respectively. The same arrangement may also exist in the *z*-direction for finite width textures. In the ***asymmetric partially textured pattern***, the textures are concentrated in only one side (left or right hand side) of the bearing. In this case, depending to the direction of sliding, the outcomes from the bearing can differ considerably. In the favoured sliding direction, the hydrodynamic load support can become significant, whilst in the opposite sliding direction; the textures may not contribute to the load carrying capacity. In the ***symmetric partially textured pattern***, the textures are concentrated in the central part of the surface so that the lengths of leading and trailing edges are higher than the edge-to-edge distance between the textures. In the ***fully textured pattern***, the textures are spread along the bearing and the lengths of leading and trailing edges are less than the edge-to-edge distance between the textures.

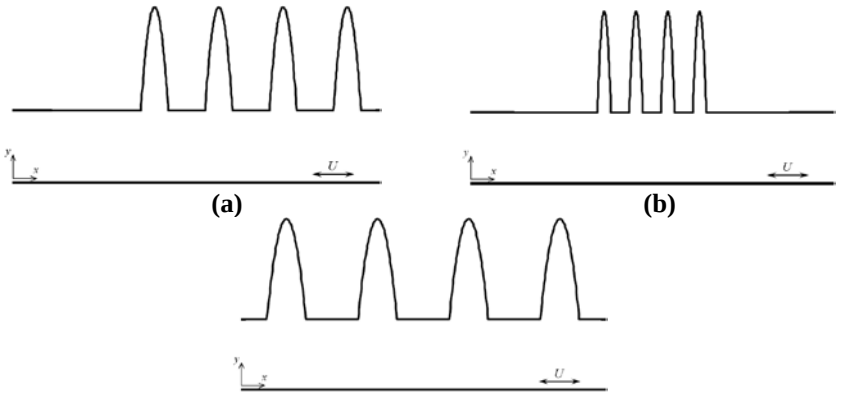

(a) **(b)**

(c)

Figure 14.7: Various texturing patterns: (a) asymmetrically partial, (b) symmetrically partial and (c) fully textured surfaces

- The type of texturing can be in the form of cavities (negative) or asperities (positive). Figure 14.6a above is a demonstration of positive type infinite width textures, whilst those in Figure 14.6b represent finite width negative type textures. In addition, the textured surfaces shown in Figure 14.7 above are all negative infinite width textures.

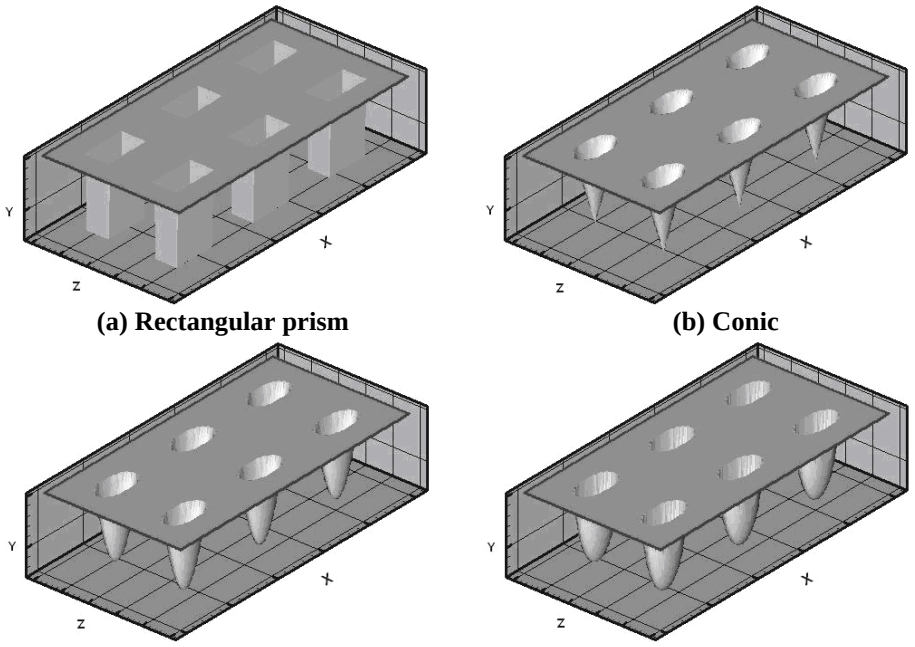

(a) Rectangular prism **(b) Conic**

(c) Paraboloid **(d) Ellipsoid**

Figure 14.8: Various texture profiles in 3D with rectangular-shape base for (a) rectangular prism with the longer lateral in the *x*-direction and an elliptical base for other texture profiles including (b) conic, (c) paraboloid and (d) ellipsoid with the major axis in the *x*-direction

- The shape of textures: In general, various texture profiles can be imagined. Different texture profiles for finite width textures are shown in Figure 14.8; including a rectangular prism, a conic, a paraboloid or an ellipsoidal profile. Equivalent type of texture profiles may also be defined in the case of infinite width textures such as rectangular, triangular, parabolic, elliptic, etc. In addition, in the case of finite width textures, the shape of the base of the

textures can be of importance as well, which one may need to include as another effective parameter in the associated computations.

- The geometrical parameters specifying the dimension of the textures: The parameters such as textures' maximum height (or depth), length (and width) of the textures, the pitch or distance between textures, the number of textures in different directions, etc. are other important parameters, particularly from the optimisation point of view. A suitable form of these parameters was defined in dimensionless forms above.
- Variations of the geometry or geometrical parameters of textures alongside the bearing: Depending on application, some geometrical parameters of textures may vary alongside the bearing's axial and/or transverse directions. For example, Figure 14.9 represents a textured bearing with constant height textures compared with the same bearing, but with uniformly variable texture heights. Such cases have been investigated in Rahmani (2009).

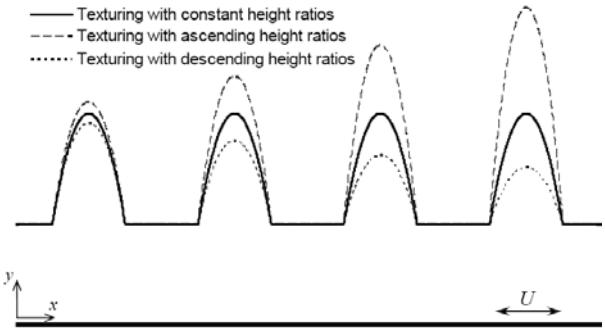

Figure 14.9: Schematic of textured bearing with contestant, ascending and descending height ratios along the bearing length

Some other parameters also exist that may be categorised as *operational parameters* and can affect the performance of a bearing in general and the textured bearing in particular. The working conditions including parameters such as variations of pressure at the boundaries or the effect of surface roughness, rheological properties of lubricant, etc are of this type. In addition, the lubrication regime in which these micro-features work e.g. hydrodynamic, elastohydrodynamic, mixed or boundary is another main parameter, which needs to be addressed. The performance of textures and the basic philosophy of employing these macro-/micro-features can be fundamentally different under different regimes of lubrication.

Another important parameter for optimisation is defining or determining an *objective function*. Two main objective functions may be defined in the analysis of the bearings in general: load capacity of the bearing and coefficient of friction. In the former case, the aim is to maximise the load capacity of the bearing, whilst in the latter minimisation of the function is of interest. Other parameters such as load capacity-to-lubricant flow rate ratio, which accounts for lubricant consumption to produce a desired hydrodynamic lift have also been suggested (Rahmani *et al*, 2010). Using an appropriate optimisation technique, a weighted objective function, which considers a trade-off between various performance parameters of a bearing may also be defined and employed.

14.11.2 Optimisation results

Typical results from an optimisation process for a symmetrically textured infinite width bearing are demonstrated in Figure 14.10. The results are obtained for a

fixed bearing length and the objective function was the total coefficient of friction of the bearing. Five texture profiles, including rectangular, trapezoidal, isosceles triangular, parabolic and elliptic in both negative and positive forms were considered. To overcome the negative effect of sharp edges in the convergency of numerical computations related to the rectangular shaped textures, the edges were considered to be slightly inclined. The trapezoidal shaped textures were also considered and isosceles with its upper lateral equal to the one-third of the lower lateral. The lengths of leading and trailing edges were set as a function of the edge-to-edge distance between the textures. Therefore, they can vary with the area density of the textures. For each texture type, profile and with different number of textures, the textures' height ratios as well as area density of textures were set as the optimisation parameters.

The range of variations of the textures' height ratio was between 1 to 5, although for the area density of textures the range of variations is ideally from 0 to 1, whilst in practice this range (especially the upper limit) may become restricted due to the computational penalty in refining the numerical mesh.

Figure 14.10a represents the obtained optimum texture height ratios in each case. As it can be seen, the variations of optimum texture height ratio with the number of textures are not very significant for higher numbers of textures. In addition, apart from negative rectangular textures, the rest of negative type textures have higher optimum height ratios than the positive ones. For the negative textures, the triangular and rectangular textures have the highest and lowest optimum height ratios, whilst the rest have very close optimum values. For the positive textures, the optimum values for different profiles are closer to each other in general and a similar pattern can also be observed except for the positive elliptic textures, which have the lowest optimum values at higher numbers of textures.

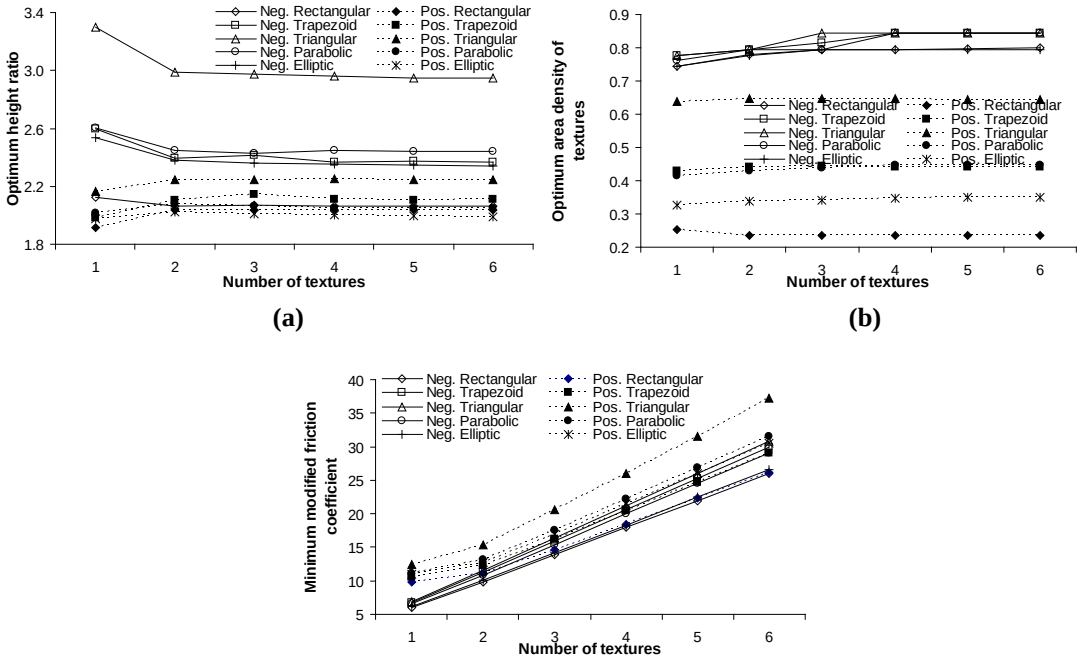

Figure 14.10: Optimum (a) height ratio and (b) area density of textures as well as (c) resulting minimum modified friction coefficients for a symmetrically textured infinite width bearing with various texture types, numbers and profiles based on minimisation of modified friction coefficients

The corresponding optimum area densities demonstrated in Figure 14.10b show distinctively the higher, but very close values for negative textures, which slightly increases at the lower numbers of textures. For this type of textures, it seems that the shape of textures has weak influence on the optimum area density of the textures. On the other hand, for the positive textures, unlike their negative counterparts, the textures' profiles have significant influence on the optimum area density values.

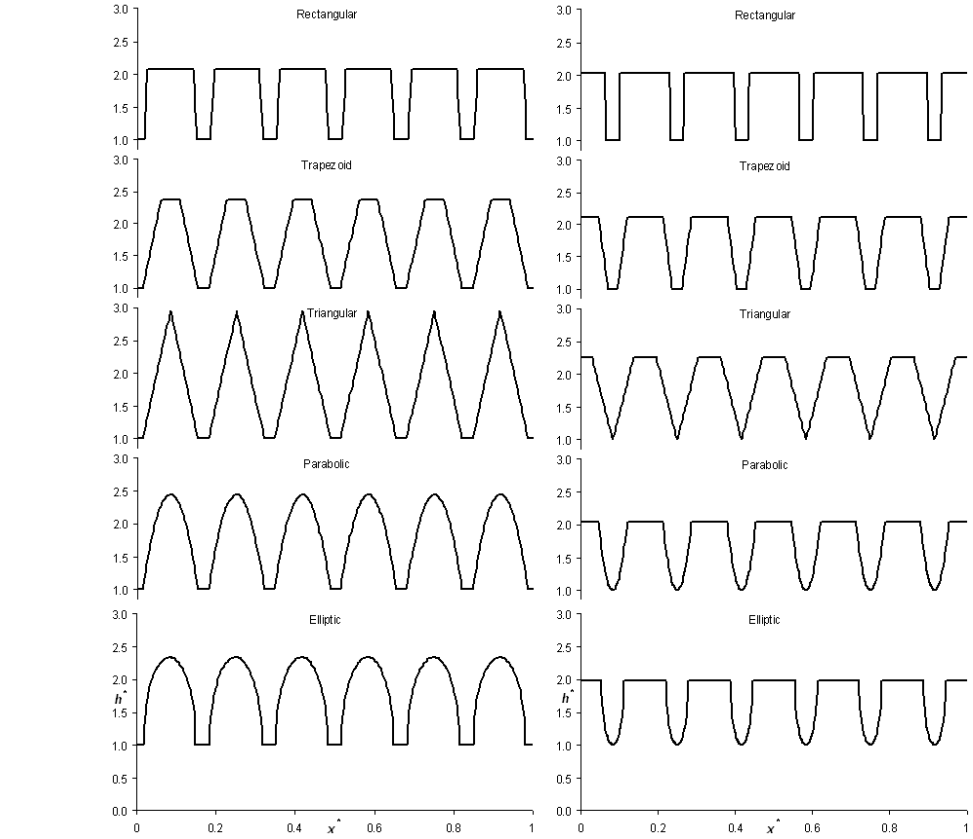

(a) Negative type textures **(b) Positive type textures**

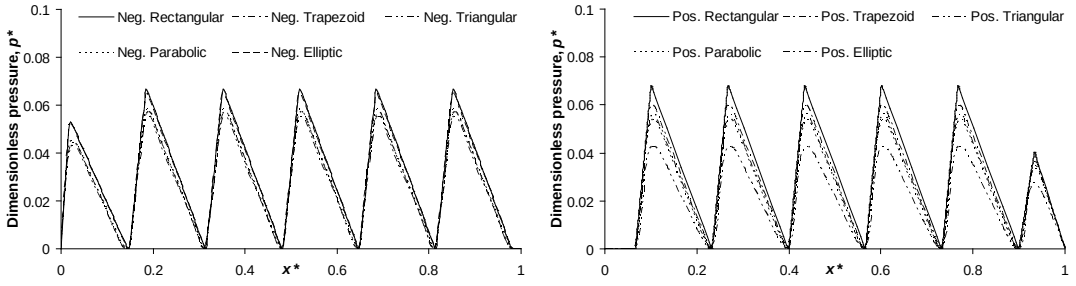

(c) Negative type textures **(d) Positive type textures**

Figure 14.11: The optimised textured bearings with (a) negative and (b) positive textures and correspondent pressure distributions for (c) negative and (d) positive textures at texture number of six for partially texturing pattern

Comparing the performance of the studied textures, based on the coefficient of friction, shown in Figure 14.10c, indicates the lowest coefficient of friction results for the negative rectangular and elliptic features, as well as positive rectangular (at higher number of textures) textures, whilst the positive triangular textures prove to be the least favoured of all. It can also be seen that the coefficient of friction increases as the

number of textures increase. In addition, the distinction between the performances of the different textured profiles slightly increases as the number of textures rises.

Figure 14.11a and b compare the obtained optimum configuration for the studied textured surfaces with six textures for negative and positive types respectively. In addition, the corresponding dimensionless pressure distribution for each case is shown in Figure 14.11c.

A similar approach can be employed for the optimisation of textured surfaces, comprising finite width textures. However, it is noted that some extra parameters may have to be considered in the case of finite width textures such as the aspect ratio of the textures' base, the lengths of the lateral edges, distance between textures, etc.

A comparison between the performance of infinite and finite width textures in their optimum configuration is given in Figure 14.12 for various number of textures, types and profiles. To obtain these results, the load capacity was set as the objective function and a fully textured pattern was considered in both cases, whilst the base aspect ratio for the finite width textures was set to unity. In addition, the area density for infinite width and the axial area density for finite width textures were equal. Therefore, textures' height ratio was the only optimisation parameter. In order to reduce CPU times, only half of row of textures in the axial direction were considered (corresponding to the A-A′ line in Figure 14.3) and the results obtained for the load capacity were then doubled. Furthermore, the bearing edge in the lateral direction was also set equal to the bearing leading (and therefore, trailing) edges in the axial direction. Thus, the final results for the load capacity of the finite width textures was in fact for a single row of textures in the axial direction including the effect of lateral edges.

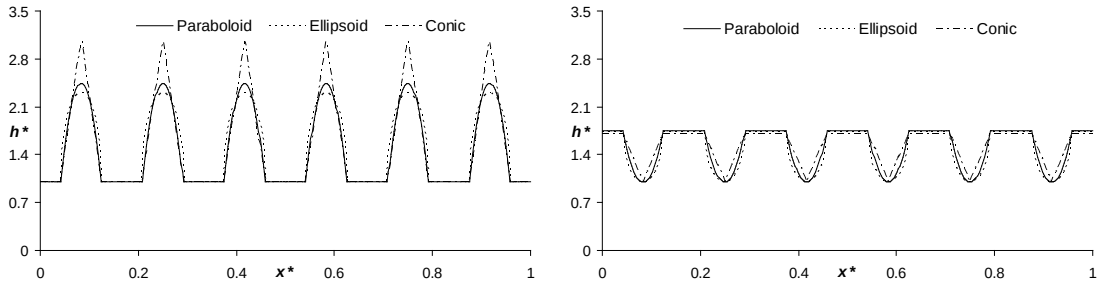

(a) Negative type textures **(b) Positive type textures**

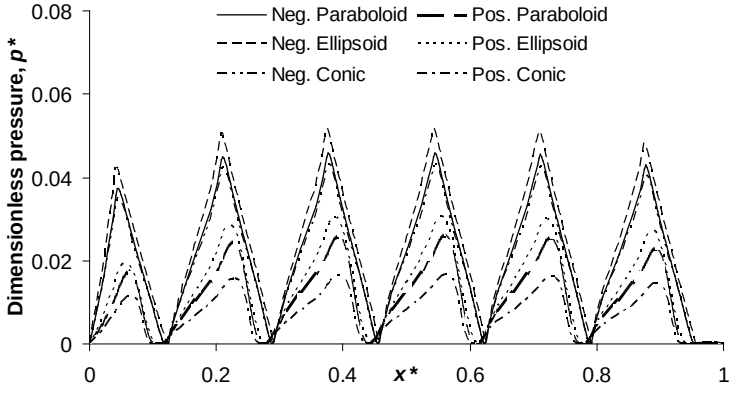

(c)

Figure 14.12: The optimised textured bearings with (a) negative and (b) positive dimples and (c) correspondent pressure distributions at texture number of six for fully texturing pattern

A cross-sectional view of the optimum configurations for the studies of 3D textures along the axis of symmetry are presented in Figure 14.12a and b for negative and positive type textures respectively, with six textures. As it can be seen, the optimum height ratios for negative textures vary more with the profile of the texture, when compared with those obtained for positive textures. As a result, it is seen that for a given texturing pattern, the optimum height ratio for the positive textures remains almost independent of their profile. In addition, in the case of negative textures, although the conic textures demand the highest optimum height ratios, they still seem to have the lowest load carrying capacity as is shown in Figure 14.12c which shows the corresponding dimensionless pressure distribution for each case along the axis of symmetry. As this figure indicates, although the profile of the textures does not have any considerable effect on the optimum height ratios for the positive textures, its effect on the performance of the bearing is relatively more significant than that of negative textures.

Figure 14.13a compares the performances (in terms of maximum attainable load capacities) of various infinite and finite width negative texture profiles at their corresponding optimum height ratios and with different number of textures. The results for the infinite width textures were obtained in the same manner as discussed above for their finite width counterparts. As it can be seen, for both cases the performance reduces as the number of textures increases. For lower number of textures the infinite width textures show higher load carrying capacity although as the number of textures increases, the difference in the results becomes less pronounced. It is also noted that for the finite width textures, the ellipsoidal textures have the highest load carrying capacities, whilst the conic ones are the poorest.

For the positive type textures, the gap between the maximum load capacities, in general, for infinite width textures and those for finite width ones are higher as is shown in Figure 14.13b. However, similar to the negative textures, this difference reduces as the number of textures grows. In addition, the infinite width textures seem to be more sensitive to the variations in the number of textures. A similar trend for the performances of the infinite width textures in terms of their shapes can be observed as was in the case of negative types.

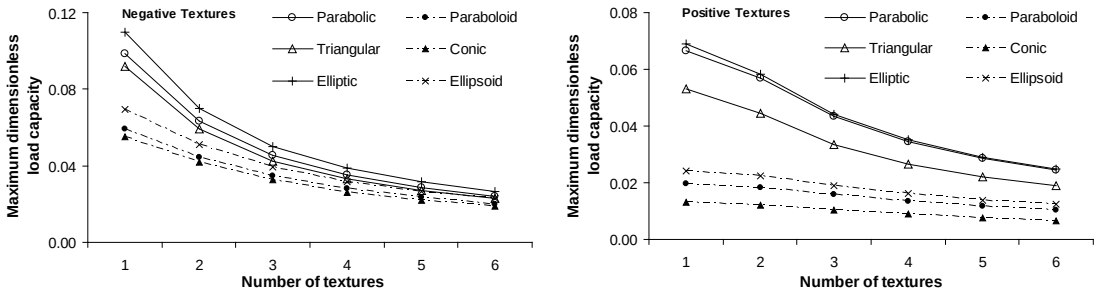

(a) **(b)**

Figure 14.13: Comparison of maximum dimensionless load capacities for infinite and finite width textures in fully texturing pattern

Considering the given results in Figure 14.13, the advantages of employing the infinite width textures over finite width textures is obvious. The reason for this is simply that in the case of finite width textures, since the lateral distance between textures is a flat surface, therefore, it will not contribute to the production of the hydrodynamic lift, when the bearing's surfaces slide relative to each other. In fact,

any build-up of hydrodynamic pressure in that region is as a consequence of the existence of textures.

14.12 Application of the optimum results in the piston-ring/cylinder liner contact

The lubrication of the piston-ring/cylinder contact is of main interest in the study of the tribology of IC engines. In this regard, the top ring has attracted much the attention (see Chapter 15). This is because the contribution of top ring to the frictional losses in the piston and piston-ring/cylinder liner contact is the highest. Investigations show that although the top ring works in the hydrodynamic regime of lubrication at mid-stroke, this usually turns to mixed (or partial) lubrication regime (and even boundary lubrication in the case of heavy-duty diesel engines) near TDC and BDC with the consequent increase in friction and wear. This is because in the mixed regime of lubrication, the asperities of ring and liner surfaces are in contact (see Chapters 2 and 3). Considering the conventional Stribeck diagram shown in Figure 14.14, the *ideal* regime of lubrication for the piston ring is the boundary between hydrodynamic and mixed lubrication regimes. Therefore, an ideal working condition for a piston ring would be the case in which the oil film thickness in the mid-stroke is reduced in order to minimise lubricant consumption and the hydrodynamic friction force, whilst it is sufficiently thick near the TDC and BDC, so that asperity contact is avoided as much as possible.

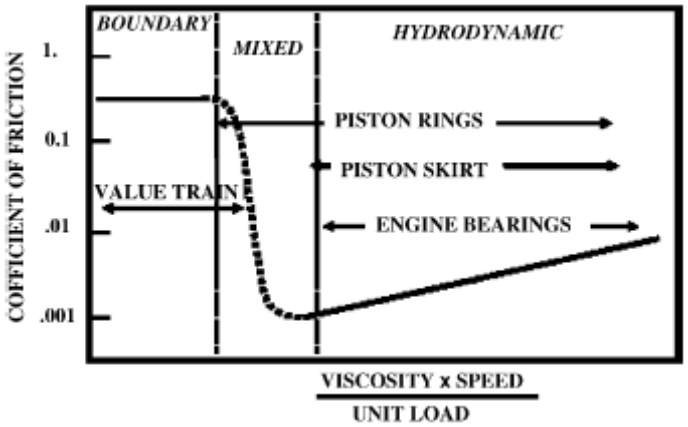

Figure 14.14: The Stribeck diagram based on Sommerfeld parameter (Tung and McMillan, 2004)

In this section, a comparison between the performances of conventional untextured barrel-shaped top ring profile and the optimised textured flat surfaces is made.

The general family of convex (converging-diverging) bearing surface profiles are defined as follows:

$$h(x) = h_m + h_R\left(2\frac{|x|}{L}\right)^n \tag{14.32}$$

in which, h_R is the height of curvature and n may be considered as the *bearing shape power*. A parameter called *crown height ratio* for this kind of bearings can also be defined as follows:

$$\zeta = 1 + \frac{h_R}{h_m} \tag{14.33}$$

Considering n=2, equation (14.32) would result in a parabolic profile, which is usually employed to approximate the piston top ring profile with sufficient accuracy (Jeng, 1992 and Baek *et al*, 2005, Mishra *et al*, 2009) and is also called the barrel-shaped profile. In this case, the bearing surface profile may be written as follows (see Figure 14.15):

$$h(x) = h_m + qx^2 \quad \text{where,} \quad q = \frac{4h_R}{L^2} \tag{14.34}$$

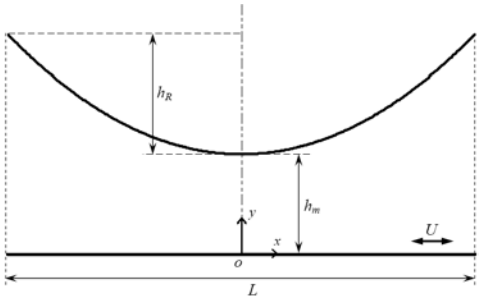

Figure 14.15: Schematic of a slider bearing with parabolic surface profile

An investigation into the optimisation of convex shaped bearing profiles shows that in the absence of a pressure difference between the bearing ends, n=2 is the optimum shape power for convex bearing families as described above. In this case, the optimum crown height ratio of ζ_{opt}=2.2 would provide the maximum dimensionless load capacity of $(W_H^*)_{max}\approx$0.0637. In addition, by considering ζ_{opt}=2.6, the minimum modified friction coefficient of $\eta'_{min}\approx$12.53 can be achieved (Rahmani, 2009).

Since the working conditions are time-dependent (transient), therefore, one needs to solve the transient Reynolds equation in the conjunction with the dynamic force balance equation as were introduced earlier. For the barrel-shaped ring profile, ζ_{opt}=2.2, which provides the highest load capacity. This is the case considered here. In addition, two texture types and profiles of negative parabolic and positive triangular were employed for comparison purposes. In both cases, a fully textured pattern was utilised. The optimum results for this texturing pattern have already been presented above. In order to reduce the CPU time, a 1D/2D model with only three textures was investigated. The values of the parameters that were used for the study were r^*=14.87, ω=1145.0rpm, δ_0=3.72E-4, F^*=1.24E+3, Λ_ω=3.33E-4, Λ_M=1.25E+8, and ι=1.0E-3.

A fourth-order Runge-Kutta approach is employed for this purpose (see e.g. Gerald and Wheatley, 1992 or Burden and Faires, 1997). Although the results for a full engine cycle; i.e. θ=0 to 720°, are of interest, some extra crank angles should also be considered in order to achieve a fully periodic solution. For the current simulations, the termination condition was achieved after around fifty iterations starting from the second period.

In addition, since the optimum height ratio for the textured surfaces and also the optimum crown height ratio for the barrel-shaped ring profile were introduced, based on the minimum film thickness, the solution approach described above needs to be repeated until the desired minimum clearance is achieved. Thus, at the start of the analysis, an initial guess for the minimum film thickness is made and the optimum height for the textures and the crown height for the ring are calculated. Once the solution is completed, the predicted minimum film thickness is used to recalculate the optimum heights for the ring and the textures. This is repeated until the difference in the obtained minimum clearances between two successive solutions becomes meets

the stated criterion. In the studied cases, the final solution was achieved usually after four iterations, as beyond that there was no significant change in the attained minimum clearance. The variations of minimum dimensionless clearance for five solution stages in the case of barrel-shaped ring profile are shown in Figure 14.16. It should be noted that in this figure and in the following figures the film thickness is non-dimensionalised, based on an initial guess for the minimum clearance.

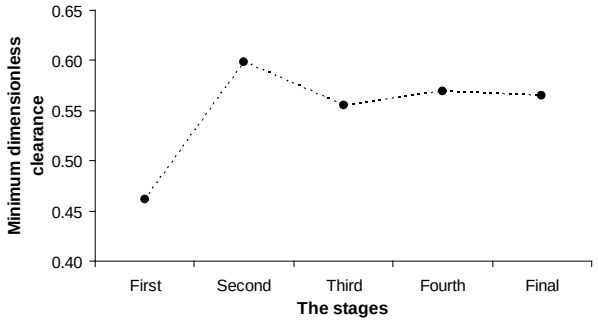

Figure 14.16: The minimum dimensionless clearance at each solution stage

Figure 14.17 shows the obtained values for the minimum clearances in the studied optimum cases in the final stage of iteration for a full four-stroke cycle of the engine. As it can be seen, the optimum positive triangular textures produce lower clearances at the mid-stroke, whilst the trade-off is the lower film clearance at and near the TDC and BDC, compared with the barrel-shaped ring profile. On the other hand, the optimum negative type parabolic shaped textures have the lower film thickness in the mid-stroke, compared with to the optimised barrel-shaped piston ring profile, whilst producing a higher film thickness at and near the TDC and BDC. The results in this figure show both the importance of type and shape of textures, as well as the effectiveness of textured surfaces, compared with the usual barrel-shaped piston rings.

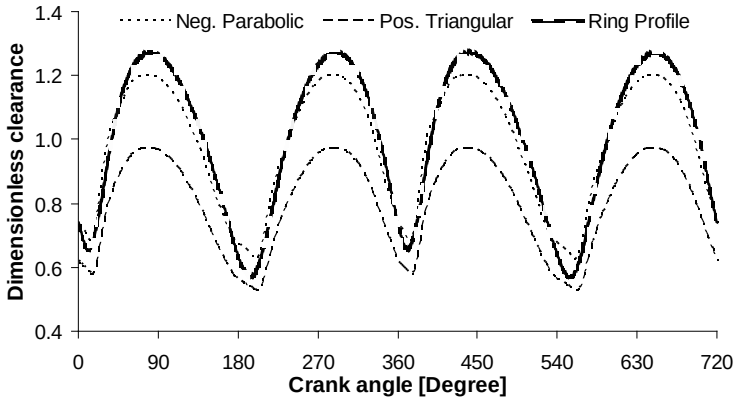

Figure 14.17: The minimum dimensionless clearance at the final stage for the studied optimum textured and untextured ring profiles

Here an important question may arise about the effect of squeeze velocity on the obtained optimum values since the optimisation was conducted based on the steady state form of Reynolds equation, neglecting the squeeze film effect. In Figure 14.18 the variations of piston axial velocity, minimum film thickness and the squeeze velocity with the crank angle for a barrel-shaped ring profile for the full four-stroke of an IC engine is shown. In this figure, the results for sliding and squeeze velocities are

scaled in the range of [-1,1] and for minimum film thickness in the range of [0,1] for the sake of demonstration.

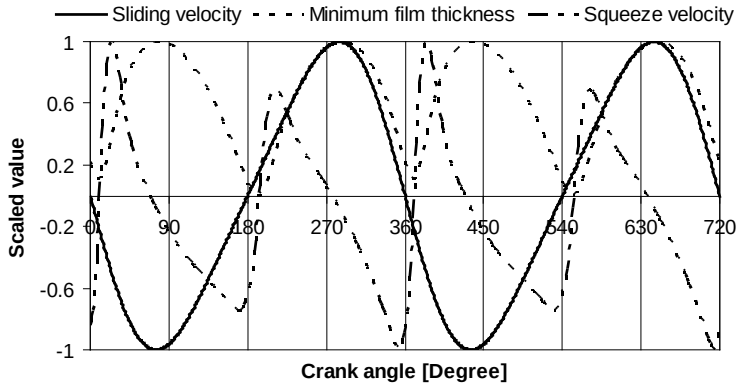

Figure 14.18: The variations of dimensionless squeeze velocity with the crank angle for barrel-shaped piston ring profile

As it can be seen in Figure 14.18, the squeeze velocity has its absolute minimum value at the mid-strokes as well as at the TDCs and BDCs. Therefore, one can observe that the squeeze velocity has a small influence in these regions and hence, the obtained optimum values from steady state analyses are a good representation. This is in line with the fact that the original aim of optimisation was to gain the highest possible performance at the crucial points of an IC engine cycle, (i.e. TDCs and BDCs).

14.13 Conclusions

From hydrodynamic lubrication point of view, the performance of the textured surfaces reduces by increasing the number of textures in the axial direction. Therefore, for a slider bearing working under full fluid film lubrication, the number of textures should be as low as possible. For bearings, which may work in other lubricating regime(s) in all or part of their sliding course or encountering lubricant starvation, an optimum number of textures that makes a trade-off between their hydrodynamic performance and their role as the oil reservoirs and debris traps should be sought with further investigations.

For a lower number of textures, the obtained optimum values for texture height ratio, area density and/or optimum textured area ratio can vary in different ways, dependent on the parameters such as texture types and/or profiles. Nevertheless, as the number of textures rises, the trend(s) in the variations of the optimum parameters with the number of textures for a given texture type and profile can be predicted since the variations become uniform and steady.

For infinite width negative type textures, the rectangular (and with a minor difference the elliptical) shape grooves are the best whilst with the positive side, the rectangular ones are the best by far. In both negative and positive type textures, the triangular shape grooves are the worst. In addition, the negative infinite width textures seem to have better performance than the positive ones.

For finite width textures, those with ellipsoidal and conical profiles were found to perform the best and worst respectively, in both positive and negative forms. However, based on the obtained results for the infinite width textures, it is expected that the rectangular prism shape textures in their optimum configuration perform even better than the ellipsoidal ones. In addition, the optimised negative form of the finite

width textures provided better performances, compared with their positive counterparts.

It was observed that for textures in positive form, the infinite width variety have certain advantages over the finite width ones in general. Although the same is true for the negative type textures, the difference is less pronounced than in the case of positive textures and it reduces further as the number of textures increases.

The obtained optimum results based on steady state form of Reynolds equation can be applied to enhance the lubrication conditions at the critical points near TDC and BDC reversals and/or control the lubricant flow through mid-strokes in IC engines, as the squeeze velocity becomes zero at such instances. In fact, employing the appropriate *optimally designed* textures, based on the critical conditions in the vicinity of TDC and BDC, not only one can enhance the lubrication condition by increasing the minimum clearance, it can also control the lubricant flow through the mid-strokes by minimising the minimum clearance there. Therefore, the appropriate and optimised textures in the piston-ring/cylinder liner contact could be more beneficial than employing the common barrel-shaped piston rings from tribological point of view.

14.14 References

Alberdi A., Merino S., Barriga J., Aranzabe A. (2004) **Microstructured Surfaces for Tribological Applications,** *Tribology and Lubricant Engineering, 14th International Colloquium Tribology; Esslingen, January 13-15, Germany*

Aldajah S., Ajayi O.O., Fenske G.R. (2005) **Investigation of Scuffing Resistance and Tribological Performance of Laser Modified Surfaces,** *The 6th Annual U.A.E. University Research Conference, College of Engineering, April, UAE, pp. Eng.224-232*

Andersson P., Koskinen J., Varjus S., Gerbig Y., Haefke H., Georgiou S., Zhmud B, Buss W. (2007) **Microlubrication Effect by Laser-Textured Steel Surfaces,** *Wear, Vol. 262, pp. 369-379*

Anno J.N., Walowit J.A., Allen C.M. (1968) **Microasperity Lubrication,** *Journal of Lubrication Technology, Transactions of the ASME, Vol. 90, pp. 351-355*

Anno J.N., Walowit J.A., Allen C.M. (1969) **Load Support and Leakage from Microasperity-Lubricated Face Seals,** *Journal of Lubrication Technology, Transactions of the ASME, Vol. 91, pp. 726-731*

Baek J.S., Groll E.A., Lawless P.B. (2005) **Piston-Cylinder Work Producing Expansion Device in a Transcritical Carbon Dioxide Cycle: Part II: Theoretical Model,** *International Journal of Refrigeration, Vol. 28, pp. 152-164*

Barrell D.J.W., Priest M., Taylor C.M. (2000) **The Axial Motion of the Piston Ring in the Top Ring Groove of a Gasoline Engine,** *Proceedings of the 27th Leeds-Lyon Symposium on Tribology, Lyon, France*

Blatter A., Maillat M., Pimenov S.M., Shafeev G.A., Simakin A.V., Loubnin E.N. (1999) **Lubricated Sliding Performance of Laser-Patterned Sapphire,** *Wear, Vol. 232, pp. 226-230*

Blau P.J., Qu J. (2004) **Laser Surface Texturing of Lubricated Ceramic Parts,** *FY 2004 Progress Report on Heavy Vehicle Propulsion Materials, pp. 123-128, URL: http://www1.eere.energy.gov/vehiclesandfuels/pdfs/hv_propulsion_04/4k_blau-laser.pdf*

Booker J.F. (1988) **Classic Cavitation Models for Finite Element Analysis,** *NASA Technical Memorandum No. TM-103184, pp. 39-40*

Borghi, A., Gualtieri, E., Marchetto, D., Moretti, L., Valeri, S. (2008) **Tribological Effects of Surface Texturing on Nitriding Steel for High-Performance Engine Applications,** *Wear, Vol. 265, pp. 1046–1051*

Brizmer V., Kligerman Y., Etsion, I. (2003) **A Laser Surface Textured Parallel Thrust Bearing,** *Tribology Transactions, Vol. 46, No. 3, pp. 397-403*

Burden R.L., Faires J.D. (1997) **Numerical Analysis,** *6th Edition, Brooks/Cole Publishing Co., US*

Christopherson D.G. (1941) **A New Mathematical Model for the Solution of Film Lubrication Problems,** *Proceedings of the Institution of Mechanical Engineers London, Vol. 146, Part 3, pp. 126-135*

Costa H.L., Hutchings I.M. (2007) **Hydrodynamic Lubrication of Textured Steel Surfaces under Reciprocating Sliding Conditions,** *Tribology International, Vol. 40, pp. 1227-1238*

Erdemir A. (2005) **Review of Engineered Tribological Interfaces for Improved Boundary Lubrication,** *Tribology International, Vol. 38, pp. 249-256*

Erdemir A., Ajayi L., Eryilmaz O., Kazmanli K., Etsion I. (2004a) **Superhard Nanocrystalline Coatings for Wear and Friction Reduction,** *FY 2004 Annual Report on Heavy Vehicle Systems Optimization Program, pp. 121-126, URL: http://www1.eere.energy.gov/vehiclesandfuels/pdfs/program/2004_hv_optimization.pdf*

Erdemir A., Ajayi O., Kovalchenko A., Kazmanli K., Erck R., Eryilmaz O., Fenske G. (2004b) **Laser Texturing of Materials,** *FY 2004 Progress Report on High Strength Weight Reduction Materials, pp. 71-76, URL: http://www1.eere.energy.gov/vehiclesandfuels/pdfs/hswr_2004/fy04_hswr_4c.pdf*

Erdemir A., Ajayi O., Kovalchenko A., Kazmanli K., Erck R., Eryilmaz O., Fenske G. (2005) **Laser Texturing of Propulsion Materials,** *FY 2005 Progress Report on High Strength Weight Reduction Materials, pp. 95-102, URL: http://www1.eere.energy.gov/vehiclesandfuels/pdfs/hswr_2005/fy05_hswr_4f.pdf*

Etsion I., Burstein L. (1996) **A Model for Mechanical Seals with Regular Microsurface Structure,** *Tribology Transactions, Vol. 39, No. 3, pp. 677-683*

Etsion I., Kligerman Y., Halperin G. (1999) **Analytical and Experimental Investigation of Laser-Textured Mechanical Seal Faces,** *Tribology Transactions, Vol. 42, No. 3, pp. 511-516*

Etsion I., Halperin G. (2002) and (2003) **A Laser Surface Textured Hydrostatic Mechanical Seal,** *Tribology Transactions, Vol. 45, No. 3, pp. 430-434. Also in: Sealing Technology, March 2003, pp. 6-10*

Etsion I., Halperin G., Brizmer V., Kligerman Y. (2004) **Experimental Investigation of Laser Surface Textured Parallel Thrust Bearings,** *Tribology Letters, Vol. 17, No. 2, pp. 295-300*

Etsion I. (2005) **State of the Art in Laser Surface Texturing,** *ASME Journal of Tribology, Vol. 127, pp. 248-253*

Etsion I., Halperin G., Becker E. (2006) **The Effect of Various Surface Treatments on Piston Pin Scuffing Resistance,** *Wear, Vol. 261, pp. 785-791*

Etsion I., Sher E. (2009) **Improving Fuel Efficiency with Laser Surface Textured Piston Rings,** *Tribology International, Vol. 42, pp. 542-547*

Fenske G., Erdemir A., Ajayi L., Kovalchenko A. (2003) **Parasitic Engine Loss Models,** *FY 2003 Annual Report on Heavy Vehicle Systems Optimization Program, Section IV: Friction and Wear, prepared by Argonne National Laboratory for US Department of Energy, pp. 101-106, URL: http://www1.eere.energy.gov/vehiclesandfuels/pdfs/program/2003_hv_optimization.pdf*

Gerald C.F., Wheatley P.O. (1992) **Applied Numerical Analysis,** *4th Edition, Addison-Wesley Publishing Co., US*

Gohar R., Rahnejat H. (2008) **Fundamentals of Tribology,** Imperial College Press, Singapore

Haefke H., Gerbig Y., Dumitru G., Romano V. (2000) **Microtexturing of Functional Surfaces for Improving Their Tribological Performance,** *Proceedings of the International Tribology Conference, Nagasaki, Japan, pp. 217-221*

Hamilton D.B., Walowit J.A., Allen C.M. (1966) **A Theory of Lubrication by Micro-irregularities,** *Journal of Basic Engineering, Transaction of the ASME, Vol. 88, pp.177-185*

Hoffmann K.A., Chiang S.T. (1993) **Computational Fluid Dynamics for Engineers,** *A Publication of Engineering Education System, Wichita, Kansas, USA*

Hsu S., Wang X., Chae Y., Ives L.K. (2003) **Modification of Engineering Materials for Heavy-Vehicle Applications,** *FY 2003 Progress Report on Heavy Vehicle Propulsion Materials Program, URL: http://www1.eere.energy.gov/vehiclesandfuels/pdfs/hv_propulsion/5_test_and_materials_standards.pdf*

Hsu S. (2004a) **Surface Modification of Engineering Materials for Heavy Vehicle Applications,** *FY 2004 Quarterly Progress Report for Progress Report on Heavy Vehicle Propulsion Materials, prepared by Oak Ridge National Laboratory for US Department of Energy, URL: http://www.ornl.gov/sci/propulsionmaterials/pdfs/HV_04_1.pdf*

Hsu S. (2004b) **Surface Modification of Engineering Materials for Heavy Vehicle Applications,** *FY 2004 Progress Report on Heavy Vehicle Propulsion Materials, prepared by Oak Ridge National Laboratory for US Department of Energy, pp. 205-209, URL: http://www1.eere.energy.gov/vehiclesandfuels/pdfs/hv_propulsion_04/5_test_and_materials_standards.pdf*

Hsu S., Wang X., Ives L.K., Zhang H., Liang Y., Ying C. (2005) **An Integrated Surface Modification of Engineering Materials for Heavy Vehicle Applications,** *FY 2005 Progress Report on Heavy Vehicle Propulsion Materials, prepared by Oak Ridge National Laboratory for US Department of Energy, pp. 231-235, URL: http://www1.eere.energy.gov/vehiclesandfuels/pdfs/hv_propulsion_05/5d_hsu.pdf*

Hupp S.J. (2004) **A Tribological Study of the Interaction between Surface Micro Texturing and Viscoelastic Lubricants,** *Master Thesis, Department of Mechanical Engineering, Massachusetts Institute of Technology (MIT), US*

Ike, H., Tsuji, K., Takase, M. (2002) **In Situ Observation of a Rolling Interface and Modelling of the Surface Texturing of Rolled Sheets,** *Wear, Vol. 252, pp. 48-62*

Ito H., Kaneda K., Yuhta T., Nishimura I., Yasuda K., Matsuno T. (2000) **Reduction of Polyethylene Wear by Concave Dimples on the Frictional Surface in Artificial Hip Joints,** *The Journal of Arthroplasty, Vol. 15, No. 3, pp. 332-338*

Jeng Y.-R. (1992) **Theoretical Analysis of Piston-Ring Lubrication, Part I - Fully Flooded Lubrication,** *ASME Tribology Transactions, Vol. 35, No. 4, pp. 696-706*

Kortikar S.N. (2004) **Fabrication and Characterization of Deterministic Microasperities on Thrust Surfaces,** *Master Thesis, College of Engineering, University of Kentucky, Lexington, Kentucky, US*

Kovalchenko A., Ajayi O., Erdemir A., Fenske G., Etsion I. (2005) **The Effect of Laser Surface Texturing on Transitions in Lubrication Regimes during Unidirectional Sliding Contact,** *Tribology International, Vol. 38, pp. 219-225*

Krupka I., Hartl M. (2007) **The Effect of Surface Texturing on Thin EHD Lubrication Films,** *Tribology International, Vol. 40, pp. 1100-1110*

Lisowsky, B. (2006) **Efficiency Improvement through Reduction of Friction and Wear in Powertrain Systems,** *FY 2006 Progress Report on Heavy Vehicle Systems Optimization Program, URL: http://www1.eere.energy.gov/vehiclesandfuels/pdfs/program/2006_hvsop_report.pdf*

Lu, X, Khonsary, M. (2007) **An Experimental Investigation of Dimple Effect on the Stribeck Curve of Journal Bearings,** *Tribology Letters, Vol. 27, pp. 169–176*

Lubbinge H. (1999) **On the Lubrication of Mechanical Face Seals,** *PhD Thesis, University of Twente, Enschede, the Netherlands*

Marian V. (2002) **Lubrication of Textured Surfaces,** *Proceedings of International Conference "Universitaria Ropet 2002", Mechanical Engineering, Vol. 2, October 17-19, Romania*

McNickle A.D., Etsion I. (2004) **Near-Contact Laser Surface Textured Dry Gas Seals,** *Journal of Tribology, Transactions of the ASME, Vol. 126, No. 4, pp. 788-794*

Mishra P.C., Rahnejat H., King P.D. (2009) **Tribology of the Ring–Bore Conjunction Subject to a Mixed Regime of Lubrication,** *Proceedings of the Institution of Mechanical Engineers, Part C: Journal of Mechanical Engineering Science, Vol. 223, No. 4, pp. 987-998*

Mourier L., Mazuyer D., Lubrecht A.A., Donnet C. (2006) **Transient Increase of Film Thickness in Micro-Textured EHL Contacts,** *Tribology International, Vol. 39, pp. 1745-1756*

Neves D., Diniz A.E., de Lima M.S.F. (2006) **Efficiency of the Laser Texturing on the Adhesion of the Coated Twist Drills,** *Journal of Materials Processing Technology, Vol. 179, pp. 139-145*

Pascovici M., Marian V., Gaman, D. (2004) **Analytical and Numerical Approach of Load Carrying Capacity for Partially Textured Slider,** *Proceedings of International Nanotribology Conference, Nano Sikkim II: Friction and Biotribology, November 8-12, Peeling, Sikkim, India*

Pascovici M., Cicone T., Fillon, M., Dobrica, M.B., (2009) **Analytical Investigation of a Partially Textured Parallel Slider,** *Proceedings of IMechE, Vol. 223, Part J: Journal of Engineering Tribology, pp. 151-158*

Pettersson U., Jacobson S. (2003) **Influence of Surface Texture on Boundary Lubricated Sliding Contacts,** *Tribology International, Vol. 36, pp. 857-864*

Pettersson U. (2005) **Surfaces Designed for High and Low Friction,** *PhD Thesis, Department of Engineering Sciences, Uppsala University, Uppsala, Sweden*

Pettersson U., Jacobson S. (2006) **Tribological Texturing Of Steel Surfaces with a Novel Diamond Embossing Tool Technique,** *Tribology International, Vol. 39, pp. 695-700*

Pettersson U., Jacobson S. (2007) **Textured Surfaces for Improved Lubrication at High Pressure and Low Sliding Speed of Roller/Piston in Hydraulic Motors,** *Tribology International, Vol. 40, pp. 355-359*

Pinkus O., Strenlicht B. (1961) **Theory of Hydrodynamic Lubrication,** *McGraw-Hill Inc., US*

Priest M., Taylor C.M. (2000) **Automobile Engine Tribology – Approaching the Surface,** *Wear, Vol. 241, pp. 193-203*

Rahmani R. (2009) **An Investigation into Analysis and Optimisation of Textured Slider Bearings with Application in Piston-Ring/Cylinder Liner Contact,** *PhD Thesis, Anglia Ruskin University, UK*

Rahmani R., Shirvani A., Shirvani H. (2007) **Optimization of Partially Textured Parallel Thrust Bearings with Square-Shaped Micro-Dimples,** *STLE Tribology Transactions, Vol. 50, No. 3, pp. 401-406*

Rahmani R., Mirzaee I., Shirvani A., Shirvani H. (2010) **An Analytical Approach for Analysis and Optimisation of Slider Bearings with Infinite Width Parallel Textures,** *Tribology International, Vol. 43, No. 8, pp. 1551-1565*

Rahnejat H., Balakrishnan S., King P.D., Howell-Smith S. (2006) **In-Cylinder Friction Reduction using a Surface Finish Optimization Technique,** *Proceedings of IMechE, Part D: Journal of Automobile Engineering, Vol. 220, pp. 1309-1318*

Ronen A., Etsion I., Kligerman Y. (2001) **Friction-Reducing Surface-Texturing in Reciprocating Automotive Components,** *Tribology Transactions, Vol. 44, No. 3, pp. 359-366*

Ryk G., Kligerman Y., Etsion I. (2002) **Experimental Investigation of Laser Surface Texturing for Reciprocating Automotive Components,** *Tribology Transactions, Vol. 45, No. 4, pp. 444-449*

Ryk G., Etsion I. (2006) **Testing Piston Rings with Partial Laser Surface Texturing for Friction Reduction,** *Wear, Vol. 261, pp. 792-796*

Siripuram R.B. (2003) **Analysis of Hydrodynamic Effects of Microasperity Shapes on Thrust Bearing Surfaces,** *Master Thesis, University of Kentucky, Kentucky, US*

Stachowiack G.W., Batchelor A.W. (2001) **Engineering Tribology,** *2nd Edition, Butterworth-Heinemann, US*

Taylor R.I., Coy R.C. (2000) **Improved Fuel Efficiency by Lubricant Design: A Review,** *Proceedings of the IMechE, Part J Journal of Engineering Tribology, Vol. 214, No. 1, pp. 1-15*

Tung S.C., McMillan M.L. (2004) **Automotive Tribology Overview of Current Advances and Challenges for the Future,** *Tribology International, Vol. 37, pp. 517-536*

Uehara Y., Wakuda M., Yamauchi Y., Kanzaki S., Sakaguchi S. (2004) **Tribological Properties of Dimpled Silicon Nitride under Oil Lubrication,** *Journal of the European Ceramic Society, Vol. 24, pp. 369-373*

Vermeulen, M., Scheers, J. (2001) **Micro-Hydrodynamic Effects in EBT Textured Steel Sheet,** *International Journal of Machine Tools & Manufacture, Vol. 41, pp. 1941–1951*

Wagner K., Volkl R., Engel U. (2006) **Tool Life Enhancement in Cold Forging by Locally Optimized Surfaces,** *Journal of Materials Processing Technology, Vol. 177, pp. 206–209*

Wagner K., Putz A., Engel U. (2008) **Improvement of Tool Life in Cold Forging by Locally Optimized Surfaces,** *Journal of Materials Processing Technology, Vol. 201, pp. 2–8*

Wakuda M., Yamauchi Y., Kanzaki S., Yasuda Y. (2003) **Effect of Surface Texturing on Friction Reduction between Ceramic and Steel Materials under Lubricated Sliding Contact,** *Wear, Vol. 254, pp. 356-363*

Wang X., Kato K., Adachi K., Aizawa K. (2001) **The Effect of Laser Texturing of SiC Surface on the Critical Load for the Transition of Water Lubrication Mode from Hydrodynamic to Mixed,** *Tribology International, Vol. 34, pp. 703-711*

Wang X., Kato K., Adachi K., Aizawa K. (2003) **Loads Carrying Capacity Map for the Surface Texture Design of SiC Thrust Bearing Sliding in Water,** *Tribology International, Vol. 36, pp. 189-197*

Wang Q.-J., Zhu D. (2005) **Virtual Texturing: Modelling the Performance of Lubricated Contacts of Engineered Surfaces,** *Journal of Tribology, Transactions of the ASME, Vol. 127, No. 4, pp. 722-728*

Wang X., Adachi K., Otsuka K., Kato K. (2006) **Optimization of the Surface Texture for Silicon Carbide Sliding in Water,** *Applied Surface Science, Vol. 253, pp. 1282-1286*

Wong V., Tian T., Moughon L., Takata R., Jocsak J., Stanglmaier R., Bestor T., Evans K., Quillen K. (2006) **Low-Engine-Friction Technology for Advanced Natural-Gas Reciprocating Engines,** *Annual Technical Progress Report for April 2005 to May 2006, Massachusetts Institute of Technology (MIT), submitted to Department of Energy of National Energy Technology Laboratory, US*

Yagi K., Takedomi W., Tanaka H., Sugimura J. (2008) **Improvement of Lubrication Performance by Micro Pit Surfaces,** *Tribology Online, Vol. 3, No. 5, pp. 285-288*

Yi W., Dang-Sheng X. (2008) **The Effect of Laser Surface Texturing on Frictional Performance of Face Seal,** *Journal of Materials Processing Technology, Vol. 197, pp. 96–100*

Yu X.Q., He S., Cai R.L. (2002) **Friction Characteristics of Mechanical Seals with a Laser-Textured Seal Face,** *Journal of Materials Processing Technology, Vol. 129, pp. 463-466*

14.15 Nomenclature

A_d	surface area of the base of each individual texture
a	leading edge length
B	bearing width
b	trailing edge length
d	length (diameter) of the texture
F	sum of forces in the radial direction excluding the hydrodynamic force
F_a	friction force due to asperity contact
F_G	radial friction force between groove and ring
F_v	viscous friction force
h	normal distance between two surfaces at any location and time
h_1	normal distance of the lower surface from *xz*-plane at any location
h_2	normal distance of the upper surface from *xz*-plane at any location
h_d	maximum height (depth) of the texture measured from texture's base
h_m	minimum distance between two bearing surfaces at any time
h_s	bearing surface profile without considering the minimum clearance

L	bearing length
l	edge-to-edge distance between two successive textures
l_c	connecting rod (conrod) length
m	(piston ring) mass
N	number of textures
n	shape power for convex (converging-diverging) bearing profiles
P_A	axial gas pressure force
P_a	ambient (reference) pressure
P_b	gas pressure at crankcase
P_L	radial gas pressure force exerted at the unwetted lower edge of the ring
P_R	radial component of blow-by gas pressure force
P_t	gas pressure in the combustion chamber
P_U	radial gas pressure force on the unwetted upper edge of the ring
p	pressure
Q	volume flow rate of lubricant
q	shape factor for barrel-shape bearing surface profile
R_G	axial reaction force from groove onto the ring
r	crank radius
Sp	the area density of the textures
s	instantaneous centre-to-centre distance between piston and crankshaft
T	radial force due to elastic tension
t	time
U	sliding velocity
U_1	tangential component of velocity vector of lower surface
U_2	tangential component of velocity vector of upper surface
v_p	axial velocity of piston
V_1	transverse component of velocity vector of lower surface
V_2	transverse component of velocity vector of upper surface
W_1	normal component of velocity vector of lower surface
W_2	normal component of velocity vector of upper surface
W_a	radial force due to asperity contact
W_g	weight (force)
W_H	hydrodynamic lift force (load carrying capacity)
x,y,z	Cartesian (spatial) x-, y- and z-coordinates

Greek Symbols

α	leading edge length to bearing length ratio (leading length ratio)
β	trailing edge length to bearing length ratio (trailing length ratio)
δ_0	the initial minimum clearance to bearing length ratio
ζ	crown height ratio for barrel-shape ring profile
η	friction coefficient
η'	modified friction coefficient
θ	crank angle
ι	termination condition for transient analysis

κ	textured area ratio (textured portion)
Λ	bearing number
Λ_M	dimensionless inertia parameter
Λ_ω	transient bearing number
λ	connecting rod (conrod) ratio
η_0	dynamic viscosity
Ξ	dimensionless trigonometric function for piston velocity
ξ	textures height ratio
ρ	density
φ	the bearing aspect ratio in the *xz*-plain
φ_d	the base aspect ratio of textures
ω	angular velocity of the crank

Mathematical Notations

$\approx$	approximately equal
$\in$	membership
$[a,b]$	closed interval (a and $b \in [a,b]$)
$^\circ$	degree
∂	operator for derivation for multivariable function
$\int$	operator for continuous summation (integration)
%	percent
cos	trigonometric cosine function
sin	trigonometric sine function

Superscripts

*	dimensionless form

Subscripts

$_1$	related to the lower surface of the bearing
$_2$	related to the upper surface of the bearing
$_{min}$	minimum
$_{max}$	maximum
$_{opt}$	optimum
$_x$	in the *x*-direction
$_y$	in the *y*-direction
$_z$	in the *z*-direction

Units

µ	micro-

Abbreviations

1D/2D	one/two-dimensional (quasi-two dimensional)
2D/3D	two/three-dimensional (quasi-three dimensional)
AJM	abrasive jet machining
BDC	bottom dead centre

BMI	Battelle Memorial Institute
CO_2	carbon dioxide
CPU	central processing unit
DLC	diamond-like carbon
EHD	elastohydrodynamic (lubrication)
EHL	elastohydrodynamic lubrication
FDM	finite difference method
HC	hydrocarbon emissions
IC	internal combustion
LBM	laser beam machining
LIGA	lithiographie, galvanoformung, abformung (lithography, electroplating, moulding)
LST	laser surface texturing (textured)
LUD	lower and upper decomposition
MEMS	micro-electromechanical systems
Neg	negative
NOx	nitrogen oxides
N-S	Navier-Stokes (equations)
ODE	ordinary differential equation
PDE	partial differential equation
Pos	positive
PSOR	point successive over-relaxation method
PVD	physical vapour deposition
RIE	reactive ion etching
RSS	Reynolds-Swift-Stieber cavitation model
SiC	silicon carbide
SOR	successive over-relaxation method
TDC	top dead centre
TiCN	titanium carbonitride
TiN	titanium nitride
US	United States
UV	ultra violet